School of Computer Science
Faculty of Science and Engineering
University Of Nottingham
Malaysia

UG FINAL YEAR DISSERTATION REPORT

– Hybrid Quantum Convolutional Neural Network –

Student's name : Hoo Kai Ping
Student Number : 20411482
Supervisor Name : Tan Chye Cheah
Year : 2025

SUBMITTED IN PARTIAL FULFILLMENT OF THE REQUIREMENTS FOR THE AWARD OF BACHELOR OF SCIENCE IN COMPUTER SCIENCE WITH AI (HONS)
THE UNIVERSITY OF NOTTINGHAM

- Hybrid Quantum Convolutional Neural Network -

Submitted in May 2025, in partial fulfillment of the conditions of the award of the degrees B.Sc.

- **Hoo Kai Ping** -
School of Computer Science
Faculty of Science and Engineering
University of Nottingham
Malaysia

I hereby declare that this dissertation is all my own work, except as indicated in the text:

Signature 

Date 4/5/2025

Acknowledgements

I would like to express my deepest gratitude to my supervisor, Dr. Tan Chye Cheah, for his unwavering guidance, encouragement, and expertise throughout the duration of this project. From the earliest stages of conceptualizing a hybrid quantum–classical neural network to the final drafting of this dissertation, Dr. Tan provides insightful feedback on the Structured Variational Quantum Circuit design, ENEQR encoding strategy, and Fourier expressivity analysis greatly sharpened the clarity of this work.I am also grateful for Dr. Tan's patient mentorship in navigating the challenges of quantum circuit simulation—especially under the constraints of limited computational resources, which enabled me to stay focused and motivated even when progress was slow. His suggestions for troubleshooting convergence issues and optimizing the quantum–classical training loop were instrumental in achieving the performance results reported here.

This dissertation would not have been possible without the mentorship and generosity of Dr. Tan Chye Cheah, to whom I extend my heartfelt thanks.

Abstract

This dissertation presents the design, implementation, and evaluation of Hybrid Quantum Convolutional Neural Networks (HQCNNs) that integrate structured variational quantum circuits (SVQCs) into a classical convolutional framework to enhance image classification performance. Motivated by the limitations of purely classical CNNs in capturing complex, high-dimensional correlations and the instability of traditional random variational quantum circuits, we propose a series of four HQCNN architectures that progressively increase quantum encoding precision, entanglement topology, and classical post-processing depth. Classical baselines based on a two-layer LeNet-style CNN were first established on the MNIST dataset to serve as reference points. Each HQCNN replaces one convolutional layer with a quanvolutional layer: 2×2 image patches are encoded via an Enhanced Novel Enhanced Quantum Representation (ENEQR) scheme into small qubit registers, processed by an SVQC, and measured to yield quantum feature maps. Version 1 employs a simple linear entanglement chain over 5 qubits (q = 2), while Version 2 adds wrap-around entanglement to form a closed-loop topology. Version 3 augments the classical head with deeper, batch-normalized multilayer perceptrons, and Version 4 increases encoding fidelity to q = 4 (7 qubits per patch). All models were trained end-to-end using the Adam optimizer and cross-entropy loss over 10 epochs on a PennyLane simulator. The results show that Version 4 has the best test accuracy of 96%, surpassing prior HQCNN benchmarks with substantially fewer quantum resources and training epochs. Fourier Expressivity Analysis reveals that richer entanglement and encoding broaden the circuits' harmonic spectra, correlating with enhanced representational capacity.

Contents

Chapter 1

Introduction

Convolutional Neural Networks (CNNs) have evolved rapidly in the field of image classification, as they are excelled at discerning subtle features by stacking multiple layers of kernels, non-linearities, and pooling operations (L. Chen et al., 2021). Their success in benchmark datasets is widely recognized, and they have become the main learning method in computer vision (Al-Saffar, Tao, & Talab, 2017). However, as the complexity and amount of data increases, some challenges emerged for CNNs such as massive computational resources, difficult training for high-dimensional data, limits of classical frameworks to capture large-scale correlations, and so on (Cloirec, 2023).

Facing these challenges, quantum computing emerged as a promising solution. Quantum computing uses principles in quantum mechanics, such as superposition, entanglement, and quantum parallelism in information processing (Gill et al., 2024). This potentially makes it possible for quantum computers to solve problems much faster compared to classical computers. Problems that take years for a classical computer to solve may be solved by Quantum Computers in considerably shorter time (B. Liu, Ortiz, & Cirak, 2024). Quantum Machine Learning (QML) has emerged and offers promising performance gains in quantum-enhanced models in the field of machine learning (Huang et al., 2021; Martín-Guerrero & Lamata, 2022). Quantum hardware exists only in small-scale versions due to the present limitations of technology, hence, is unable to perform very complex calculations since the number of qubits available is too little (Cerezo, Verdon, Huang, Cincio, & Coles, 2022).

1.1 Motivation

An alternative approach will be hybrid versions: quantum-classical models. Hybrid Quantum Convolutional Neural Networks (HQCNNs) represent a measured step in this direction (Fan, Shi, Guggemos, & Zhu, 2024). Such models will merge the strengths of quantum and classical computing and do not need to convert the whole structure of CNN into a quantum model (H. Liu et al., 2023). These models replace the convolutional layer with a quantum convolutional layer, also known as a quanvolutional layer (Jeong et al., 2023). Instead of applying linear filters and non-linear activations directly to the pixel values, HQCNNs map these features into a quantum state and then process them through Variational Quantum Circuits (VQCs) (Rizvi, Ulum, Asif, & Shin, 2023). These quanvolutional layers act directly on the qubits which encode the classical information by drawing inspiration from superposition and entanglement to enable richer and more flexible representations of the decision boundaries (Singhal & Joshi, 2024). HQCNN aims to harness the power of quantum computing to overcome the challenges and limitations faced by current CNNs, which might accelerate their training process to navigate across complex data landscapes better than CNNs.

To facilitate the mapping from classical image data to qubits, this project approaches it using Enhance Novel Enhanced Quantum Representation (ENEQR). ENEQR provides an efficient encoding scheme to enable the translation of pixel intensities, feature maps, or other pre-processed values into quantum state in such a way that the structural information from the image is preserved (Nasr, Younes, & Elsayed, 2021). This method ensures that the quanvolutional layer processes a well-structured quantum input instead of a random scattering of amplitudes. This project is motivated by the imperative to transcend the intrinsic limitations of CNNs which are data hunger, computational overhead, and high-dimensional scaling by exploiting the unique strengths of quantum computing.

1.2 Problem Statement

The Variational Quantum Circuit (VQC) forms the basis of the quanvolutional layer. The traditional approaches in this direction have usually given rise to random circuit

structures, hence the name Random Variational Quantum Circuits (RVQCs). RVQCs use quantum gates and parameters that are randomly initialized . Therefore, they can suffer from unpredictable convergence behavior during training, frequently becoming trapped in saddle points or spurious local minima that impede effective optimization (Zhuang, Cunningham, & Guan, 2024). When present, this randomness sometimes injects a dash of expressivity, in most cases it tends to introduce variability to complicate the landscape of training (You & Wu, 2021). When hundreds or thousands of qubits and parameters are involved, these circuits exhibit the barren plateau phenomenon, wherein gradient magnitudes decay exponentially with system size or circuit depth, rendering gradient-based optimizers nearly powerless to navigate the loss landscape (Kashif & Shafique, 2024; Larocca, Thanasilp, Wang, et al., 2025). This trainability crisis is compounded by the inherent complexity of high-dimensional Hilbert spaces: as the number of variational parameters grows, the optimization landscape becomes increasingly flat and featureless, causing VQCs to stall early in training and undermining their practical utility (Anschuetz & Kiani, 2022).

While it has long been known that classical neural networks can approximate immense function classes given sufficient depth and width, quantum layers may need to widen the horizon further. The expressiveness of a quantum circuit directly influences the model's capacity to capture and learn complex patterns in the data, and its ability to represent a wide function space (Y. Wu, Yao, Zhang, & Zhai, 2021). Insufficient circuit depth or entanglement limits the function space that VQCs can represent, leading to underfitting, whereas excessive depth or random parameterization can cause overfitting and exacerbate barren plateaus, leading to suboptimal performance (Kobayashi, Nakaji, & Yamamoto, 2022; Y. Wu et al., 2021). Recent theoretical results demonstrate that reducing parameter space dimensionality by correlating gate layers or employing structured ansätze can mitigate vanishing gradients, yet naïvely random parameterized circuits remain prone to exponential proliferation of local minima and flat regions (Volkoff & Coles, 2021).

Besides, quantum data encoding faces a challenge on translating classical information into quantum states without losing spatial or intensity relationships. Traditional encoding

schemes struggle with the exponential scaling of state space and hardware constraints on qubit count and coherence times, leading to either coarse approximations or prohibitive resource demands (Rath & Date, 2024). These challenges such as barren plateaus, local minima, over-/under-expressivity, and data encoding complexity highlight the core problem: without a principled circuit architecture and encoding strategy, HQCNNs cannot reliably harness quantum advantages. Random Variational Quantum Circuits (RVQCs) inject excessive variability and lack interpretability, stalling training and muddying feature extraction. Meanwhile, classical-to-quantum encoding may either oversimplify crucial patterns or overload quantum hardware.

1.3 Objectives

This project aims to address the limitation of using RVQCs by introducing Structured Variational Quantum Circuits (SVQCs), which organizes quantum gates into a more systematic and principled patterns (S. Y.-C. Chen, 2024). This approach reduces randomness, facilitating smoother training, providing clearer interpretability, and potentially enriching the set of functions that circuits represent. This could introduce well-founded patterns that can enhance performance and understanding (Yi, Liang, & Situ, 2024). Besides, this project aims to address the limitation of expressiveness management by introducing Fourier Expressivity Analysis (FEA), which decomposes the functions produced by the quantum layers into their frequency components (Wiedmann, Periyasamy, & Scherer, 2024). This approach could measure how rich the circuit is across different functions, where a higher complexity in the frequency spectra correlates with enhanced representational power, where the circuit could disentangle more subtle patterns and adapt more fluidly to the data at hand.

The project starts the explorations of these model on MNIST dataset. MNIST dataset consist of handwritten digits which serve as a universally recognized proving ground. The project's goal is to evaluate different approaches of HQCNN's performance on MNIST against a baseline classical CNN. This investigation seeks to highlight the qualitative differences introduced by structured VQCs, and how quantum enhancements

translate into measurable improvements in learning capacity and model interpretability. Tracking these changes through Fourier expressivity metrics offers a nuanced lens to understand why and how these quantum circuits differ, rather than just whether they perform better on a simple classification test. After evaluating on MNIST dataset, the project aims to further evaluate the performance of both HQCNN and baseline classical CNN on CIFAR-10 dataset.

This project represents a step toward bridging the gap between classical and quantum machine learning by introducing structured quantum convolutional layers into the well-established CNN framework. By implementing SVQCs to replace the traditional use of RVQCs in HQCNNs, the project seeks to mitigate issues such as the training inefficiencies, optimization challenges, and lack of interpretability often associated with random circuit designs. The addition of FEA provides a quantitative approach to evaluate the functional capacity of these quantum components, enabling a deeper understanding of their contribution to the model's behaviour and performance. This project strives to explore how quantum-enhanced architectures can bring unique advantages to machine learning tasks. By addressing the limitations of current hybrid models, this project highlights the potential for quantum circuits to augment feature representation, laying the groundwork for advancements in more complex datasets and real-world applications.

1.4 Structure

This dissertation is organized into seven core chapters, each build on to develop and evaluate a structured, Hybrid Quantum–Convolutional Neural Network (HQCNN) for image classification. Chapter 1 is the introduction where it motivates the need to integrate quantum computing into classical convolutional neural networks (CNNs), we articulate the primary problem—the limitations of randomly structured variational quantum circuits and classical-to-quantum data encoding—and present the dissertation's objectives in overcoming these challenges. Chapter 2 review classical CNNs and key quantum computing concepts—superposition, entanglement, and variational quantum circuits (VQCs)—to provide necessary technical context. Chapter 3 provide details about the

experimental pipeline. Chapter 4 presents quantitative findings from training and testing on the MNIST dataset and the Fourier expressivity heatmaps for every circuit, revealing how architectural changes expand the set of frequencies—and thus functions—that the quantum layers can represent. Chapter 5 interprets the results in light of our objectives. Chapter 6 provides a personal reflection on the project's learning journey, including challenges encountered in hybrid quantum–classical integration, insights from troubleshooting gradient backpropagation through quantum layers, and how this work shaped our understanding of quantum machine learning. Chapter 7 summarize key contributions such as the SVQC design, ENEQR application, and Fourier-based expressivity framework, and their implications for near-term quantum devices.

Chapter 2

Background and Related Works

2.1 Background

Convolutional Neural Networks (CNNs) were the basis for many breakthroughs in computer vision. They use convolutional filters, activation functions, and pooling operations in succession to extract patterns and features from input data. CNNs have been successful for solving a wide range of problems. However, with increasingly complex and high-dimensional data, despite the success of CNNs, there are challenges arising in them. These include the challenge of modelling complex relationships, the computational drain it would entail, and limitations with regards to classically modeling fine details of patterns (Younesi et al., 2024).

Quantum computing introduces new principles into information processing, relying on such phenomena as superposition, entanglement, and quantum parallelism. These principles give quantum computers the potential to handle calculations in high-dimensional spaces beyond the reach for classical computers (Parmar, Parmar, Verma, Roy, & Bhattacharya, 2023). Quantum computing brought about Quantum Machine Learning (QML), combining quantum computation with classical learning techniques. QML redefines how learning tasks are performed, especially for data in high-dimensional and computationally intensive areas (Marshall, Gyurik, & Dunjko, 2023; Nagata, Diep, & Nakamura, 2022). QML had shown potential in several models, such as Quantum Support Vector machines (QSVMs), Quantum Principal Component Analysis (QPCA), and Quantum Boltzmann

Machines (QBMs) (Biamonte et al., 2016). QSVMs use quantum-enhanced kernels to perform classification tasks way more efficiently. These kernels allow for inner product calculations in high-dimensional feature spaces, which most classical SVMs struggle to explore (Suzuki, Hasebe, & Miyazaki, 2024). QPCA is a quantum version of a classical PCA; it uses quantum states to compute eigenvalues and eigenvectors. The approach had considerable computational efficiency compared to classical PCA on large-scale datasets (Lloyd, Mohseni, & Rebentrost, 2014; Y. Wang & Luo, 2024). QBMs extend the classical Boltzmann machines by including quantum sampling techniques in the modeling of complex probabilistic distributions. This capability makes QBMs advantageous for generative tasks and unsupervised learning scenarios (Amin, Andriyash, Rolfe, Kulchytskyy, & Melko, 2018; Kieferová & Wiebe, 2017).

In the realm of image classification, this was represented by Quanvolutional Neural Networks (QNNs). QNNs embed the principles of quantum computation into classical deep learning frameworks (Vu, Le, & Pham, 2024). QNNs also replace the classical convolutional layers, which allow the extraction of features from input data encoded into quantum states (Oh, Choi, & Kim, 2020). These quantum circuits operate in high-dimensional Hilbert spaces, using properties such as superposition and entanglement to capture complex correlations in data that may be challenging for classical models to identify (Zeng, Chen, Zhou, & Wen, 2019). With the discovery of QNNs came the idea of the Hybrid Quantum Convolutional Neural Networks (HQCNNs), which combined the strength of CNN with quantum computation. HQCNN replaces the classical convolutional layer with a quanvolutional one while leaving the rest of the model as classic part (Zaman, Ahmed, Hanif, Marchisio, & Shafique, 2024).

Quantum algorithms like Variational Quantum Eigensolvers (VQE) and Quantum Approximate Optimization Algorithms (QAOA) have significantly influenced the design of Variational Quantum Circuits (VQCs), which is a crucial part in QML applications. VQE was developed for solving optimization problems while QAOA was primarily used for eigenvalue problems; the key philosophies such as iterative optimization of parameters place these algorithms very strongly in the region of feature extraction and classification

tasks in QML applications (Tilly et al., 2022; Farhi, Goldstone, & Gutmann, 2014). The creation of VQCs is to make quantum circuits trainable by introducing parameterized gates whose values can be optimized during a training process. These circuits are initialized with a series of quantum gates: rotations like RX, RY, and RZ θ-dependent gates, and entangling gates like CNOT and CZ gates. The parameters of these gates, θ, are considered trainable variables that are iteratively updated by using classical optimization algorithms, such as gradient descent (Qi, Xiao, Liu, et al., 2024). The performance during the training of a VQC is measured by a loss function computed from the measurements performed on the quantum circuit (Huembeli & Dauphin, 2021).

2.2 Related Works

The Hybrid Quantum Convolutional Neural Network in (Senokosov, Sedykh, Sagingalieva, Kyriacou, & Melnikov, 2024) has presented 2 different models: HQNN-Parallel and HQNN-Quanv. HQNN-Parallel as shown in Figure 2.1, replaces the fully connected layer of a classical CNN with the Hybrid Dense Layer containing a combination of both classical and quantum layers. This hybrid dense layer uses the Parallel Parameterized Quantum Circuit (PQC). Angle embedding is utilized in the model for the encoding of classical data into quantum states. This consists of the embedding of quantum layers, variational gates, and measurement. The architecture contains trainable parameters together with entangling gates to learn the complicated patterns in the data. However, the presence of hyperparameters makes the training process challenging and computationally expensive. The ZX-calculus reduction used demonstrates that the model can be simplified without loss of its performance, and its complexity is not redundant. Additionally, Fourier expressivity analysis says the quantum layers of the model can represent a wide range of functions; in other words, it does capture the complex patterns and relationships. On the other hand, HQNN-Quanv (Figure 2.2) replaced the convolutional layer with the quanvolutional layer. In the same way as HQNN-Parallel, HQNN-Conv employs angle embedding to encode classical data into quantum states using single-qubit rotations depending on the pixel values through Ry gates. In that process, the VQC applied consists of single-qubit

rotations and CNOT gates to transform the quantum states by measuring the expectation value of the Pauli-Z operator on each qubit.

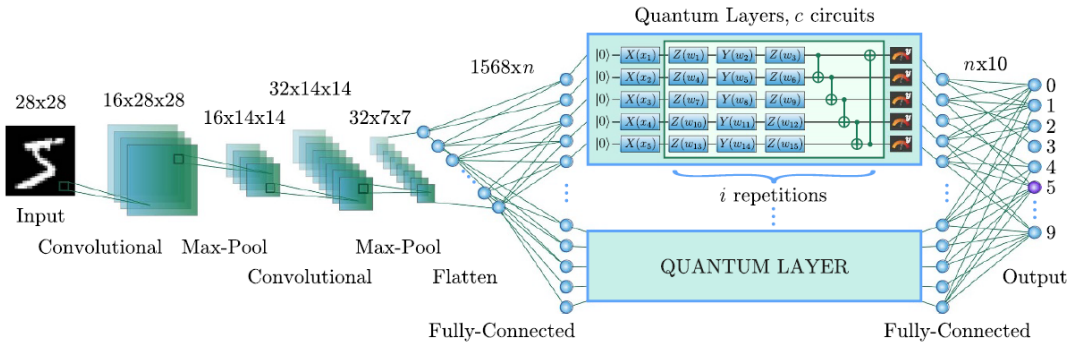

Figure 2.1: HQNN-Parallel

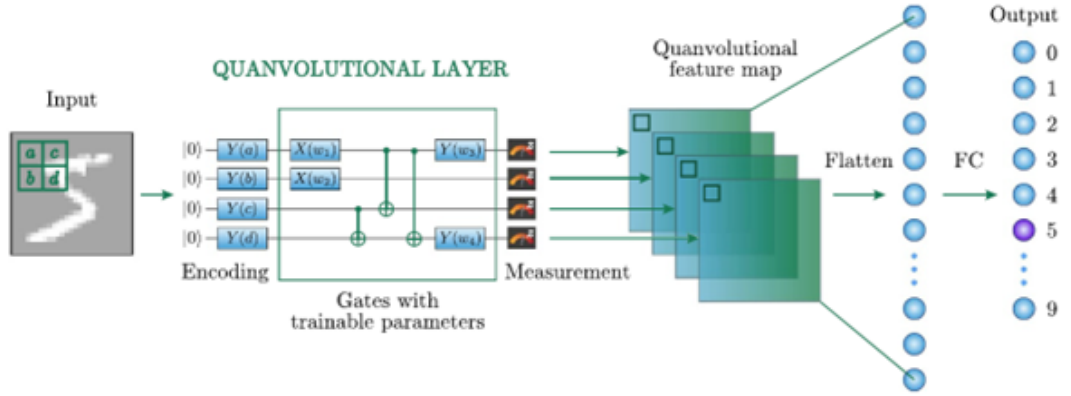

Figure 2.2: HQNN-Convo

The research in (Cong, Choi, & Lukin, 2019) proposed a fully Quantum Convolutional Neural Network (QCNN) for classification tasks. The QCNN (Figure 2.3) is composed of 2 convolutional and pooling layers, followed by a fully connected layer. The input to the QCNN is an unknown quantum state, denoted as p. The quanvolutional layer makes use of some quasilocal unitary operation U_i, applied in translationally invariant ways across the quantum system in such a way that exactly the same operation is applied to each part of it. In the quantum pooling layer, some qubits are measured, and the outcome of the measurement determines unitary rotations V_j on nearby qubits. This serves to down-sample the size of feature maps in a manner analogous to a classical pooling layer. It could be interpreted as another kind of error correction, in some sense: the quantum pooling layer applies corrective unitaries based on the measurement outcomes, trying

to keep the quantum state within the desired subspace. The fully connected layer will then be implemented as a unitary operation, denoted as F: it combines the information coming from the previous layer and generates an output that will then be decoded into a classical state. The QCNN architecture is closely related to the Multiscale Entanglement Renormalization Ansatz (MERA) tensor network, which is used to represent many-body quantum states efficiently. In a sense, the QCNN runs the MERA process in reverse. For any quantum state representable by MERA, there exists a QCNN that can be constructed to classify it perfectly by applying the inverse of the MERA circuit. The pooling layer in the QCNN is analogous to syndrome measurements in quantum error correction, it detects and corrects local errors without collapsing the wavefunction. This allows the QCNN to classify quantum states in a robust way, even when the input states are perturbed. The QCNN model can also be applied to classify quantum phases, such as detecting the 1D Symmetry-Protected Topological (SPT) phase. QCNN can identify ground states of certain Hamiltonians and, when related to a given phase.

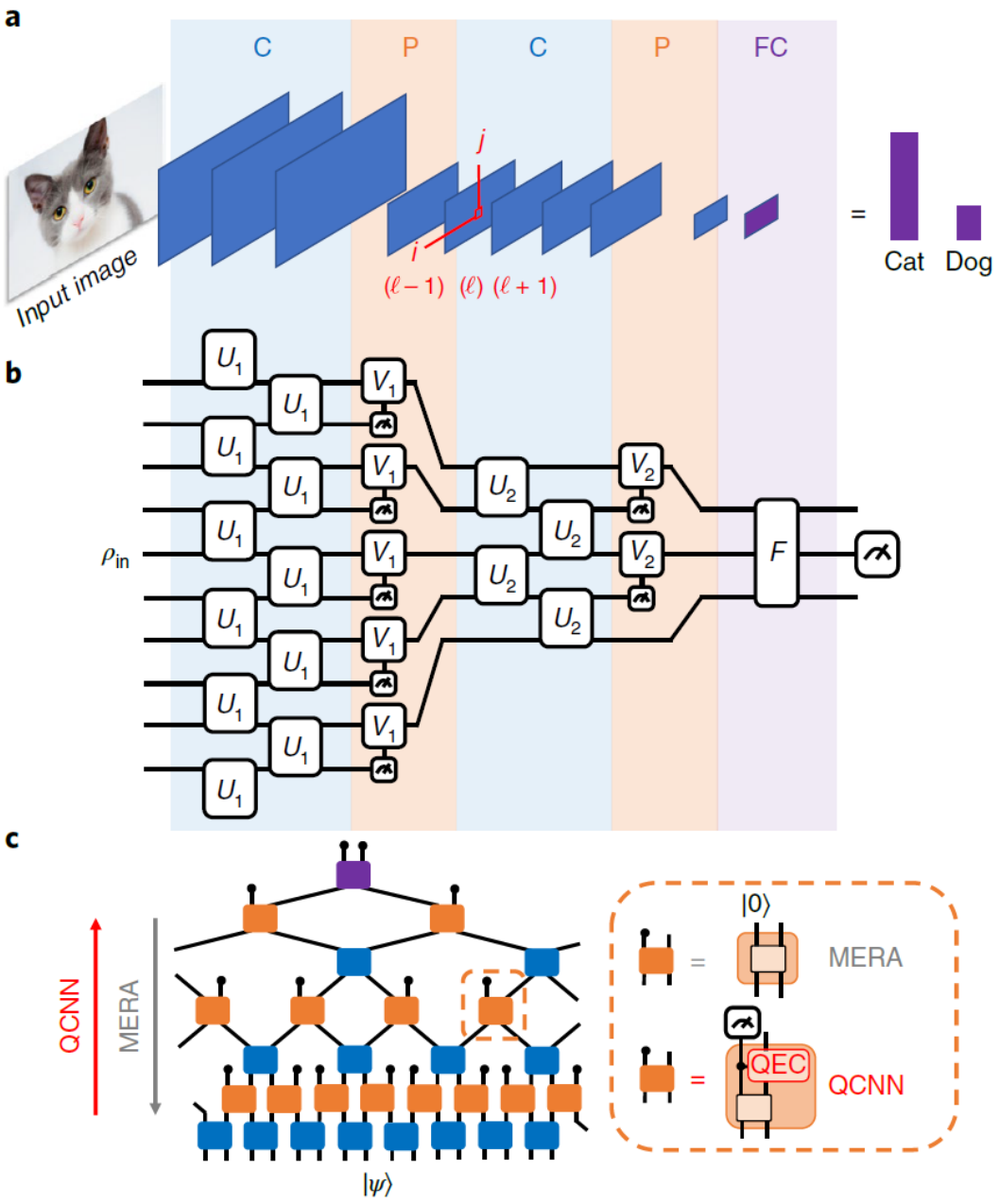

Figure 2.3: Fully QCNN

Contrasting with it, the research in (Xu, Shen, Cai, et al., 2024) proposed a Parallel Proportional Fusion (Figure 2.4) that splits the image data into 2 neural networks, namely Spiking Feedforward Neural Network (SFNN) and Variational Quantum Circuit (VQC). These are then fused after the end of the model. The SFNN would be responsible for extracting the classical features from the image input. It converts image pixels into spike trains using the Poisson Distribution, in which the firing rate of the spike stream is directly proportional to the pixel intensity. The SFNN in the fusion model is based on

the Leaky Integrate-and-Fire (LIF) neuron model, one of the simplest and most widely used models to stimulate spiking behaviour. The output is then processed using a Softmax function, where the classification result is determined by the neuron with the highest probability (firing rate). VQC is in charge of processing quantum features from the input image. The VQC uses amplitude encoding, which is the Flexible Representation of Quantum Images (FRQI), where the image data is encoded into quantum states, and encodes each pixel intensity value into the amplitude of a quantum state. At the heart of every VQC lies a parameterized quantum circuit: several layers of rotation gates with trainable parameters and entangling gates. The final state of the qubits is measured using the Pauli-Z measurement. The last part of the model is the fusion, which integrates features extracted from both classical and quantum circuits. By fusing these features, the model leverages the temporal pattern recognition capabilities of the SFNN and the complex pattern recognition potential of quantum circuits. It performs a Parallel Proportional Fusion (PPF) strategy that keeps the balance in the contribution of both classical and quantum features. It assigns a weight to both feature vectors and then combines them into one fused feature vector.

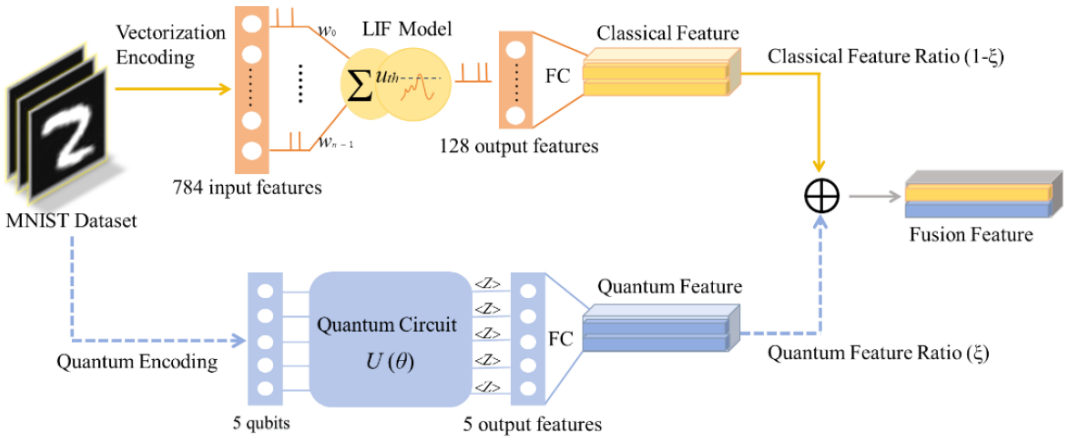

Figure 2.4: Parallel Proportional Fusion

The paper "Quantum Convolutional Neural Network Based on Variational Quantum Circuits" by (Gong, Pei, Zhang, & Zhou, 2024) explores the integration of VQCs into QCNNs, underlining their potential to outperform CNNs. The main focus of the paper is the development and application of different Structured Variational Quantum Circuits

(SVQCs). These restructure how data is processed in a quantum framework by introducing a tree-structure hybrid amplitude encoding method. Such quantum circuits have a hierarchical structuring, enabling them to transfer information effectively by reducing the likelihood of noise-induced distortions. The work applies SVQCs as a backbone for quantum convolution and pooling layers. Their proposed convolutional layers leverage an intrinsic attribute of the global entanglement inherent in SVQCs, while extracting both local and global features in the input data. This implies a huge improvement from the classical convolutional layers that allow only localized features to be extracted. The pooling is also done using SVQCs, which efficiently reduces the number of qubits by half. These pooling operations leverage the hierarchical encoding provided by SVQCs to keep the integrity of the data upon dimensionality reduction. The QCNN circuit proposed by this paper is shown in Figure 2.5. Among all the SVQCs in the paper, the best classification accuracy achieved by Circuit 6 (Figure 2.6) in the MNIST dataset will then be used in this project.

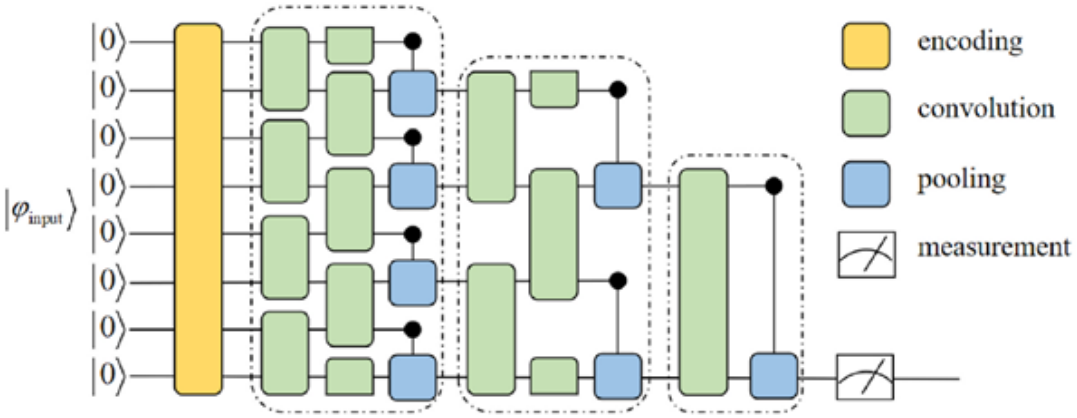

Figure 2.5: QCNN Circuit

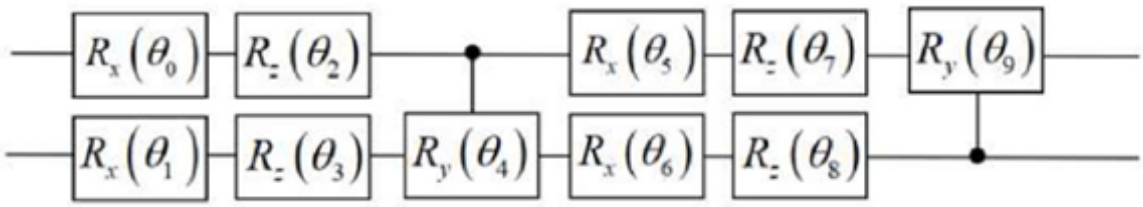

Figure 2.6: Circuit 6

2.2.1 Enhanced Novel Enhanced Quantum Representation (ENEQR)

Quantum image encoding underpins the performance of quantum-enhanced neural networks by determining how faithfully classical data—such as pixel intensities and spatial arrangements—is mapped into quantum states. The quantum encoding methods come in many flavours, such as basic encoding, superposition encoding, entanglement encoding, position encoding, and amplitude encoding (Ranga et al., 2024; Rath & Date, 2024). Flexible Representation for Quantum Images (FRQI) encodes pixel intensities into rotation angles on a single intensity qubit while using computational basis states of position qubits to index pixel locations, requiring $2n+1$ qubits for a $2^n \times 2^n$ image but demanding repeated measurements to reconstruct amplitudes accurately (Phuc, Dong, Yoshinori, & Kaoru, 2009). To achieve deterministic retrieval, the Novel Enhanced Quantum Representation (NEQR) augments FRQI by dedicating an additional q qubits per pixel to store exact grayscale values in their basis states, yielding the state

$$\frac{1}{2^n} \sum_{x,y=0}^{2^n-1} |I(x,y)\rangle \, |x\, y\rangle$$

on $2n+q$ qubits and enabling single-shot measurement of each pixel's intensity (Zhang, Lu, Gao, et al., 2013).

Despite its exact recovery and quadratic preparation-speed advantages over FRQI, NEQR's reliance on multi-controlled NOT gates and additional qubit registers incurs significant circuit depth and qubit overhead—factors that strain current NISQ devices and raise concerns about coherence and gate-error accumulation (Haque, Paul, Ulhaq, & Debnath, 2023). In this project, the Enhanced Novel Enhanced Quantum Representation (ENEQR) will be applied to do such encoding, ENEQR, proposed by (Nasr et al., 2021), is an enhanced version of NEQR by (Zhang et al., 2013). ENEQR is a hybrid approach wherein the amplitude encoding and position encoding are combined. In such a hybrid approach, it will allow the circuit to represent both pixel intensities encoded as amplitudes of the quantum state and pixel positions encoded in the superposition of position

qubits for spatial information. In ENEQR, position qubits are first placed into uniform superposition via Hadamard gates, encoding spatial indices $|x\, y\rangle$ across all pixel locations simultaneously; gray-value qubits then undergo controlled rotations and conditional bit-flips governed by the binary representation of pixel intensities, embedding exact grayscale values $|I(x, y)\rangle$ into the quantum register. ENEQR efficiently maps the classical inputs into quantum states by preserving some very crucial structural features of the data. It ensures that the quantum circuits receive meaningful input, hence optimizing the quanvolutional layers to optimally extract and process complex features. Quantum encoding methods determine the quality of the quantum state representations fed into the quantum layers (Gogeissl, Safi, & Mauerer, 2024). Unlike basic amplitude or binary encoding methods, ENEQR provides a better balance between quantum resource utilization and fidelities of feature preservation.

2.2.2 Fourier Expressivity Analysis

The limitations of parameterized quantum circuits (PQCs) is their Fourier expressivity, the ability of a circuit to represent functions as Fourier series in its classical inputs. Fourier expressivity analysis treats a parameterized quantum circuit (PQC) as a map

$$f_\Theta(x) \;=\; \sum_{\omega\in\Omega} c_\omega(\Theta)\, e^{i\,\omega x}\,,$$

where the frequency spectrum Ω is fixed by the choice of data-encoding Hamiltonians and the Fourier coefficients $c_\omega(\Theta)$ are tunable via variational parameters (Schuld, Sweke, & Meyer, 2021). By expressing PQCs in this Fourier basis, we can quantify how richly a circuit can represent functions of its classical inputs—a core measure of expressivity.

The paper "Constrained and Vanishing Expressivity of Quantum Fourier Models" gives some insights into the expressivity of Parameterized Quantum Circuits (PQCs) from the point of view of Fourier analysis (Mhiri et al., 2024). This paper presents a new, astounding correlation between the Fourier coefficients of quantum models and their encoding gates. Previous works hinted at the belief that these coefficients depended

mainly on the trainable gates inside the quantum circuits. In this paper, this assumption is broken when it shows that the encoding gates act with an order of importance equal to those of other gates. The innovative concept of frequency redundancy in the Fourier series spectrum is found. The concept of frequency redundancy, $|R(\omega)|$, defined as the number of distinct encoding-gate paths that yield the same frequency ω. They prove that, under mild randomness assumptions, the variance of each Fourier coefficient scales proportionally to its redundancy:

$$\mathrm{Var}\big[c_\omega\big] \;\propto\; \frac{|R(\omega)|}{d\,(d+1)}\,,$$

with $d = 2^n$ the Hilbert-space dimension. Crucially, they demonstrate a vanishing expressivity phenomenon: when $|R(\omega)|$ fails to grow fast enough as qubit count n increases, many Fourier modes' variances shrink exponentially, effectively removing those frequencies from the model's functional repertoire. The paper then provides guidelines for the design and optimization of PQCs. For example, to mitigate the expressivity constraints, this recommends careful choice of encoding strategies and circuit architectures. Following this paper, the encoding Hamiltonians can be designed in a way that the distribution of redundancy in them is more balanced and would thus increase the performance significantly.

Furthermore, the work in (C.-H. Wu & Yen, 2024) analyze PQCs in the context of entanglement-entropy estimation, showing that Rényi-to-von Neumann entropy continuation can be cast as a partial Fourier series in an angular parameter. They reveal that truncating high-frequency components induces a Gibbs phenomenon, which can be mitigated by projecting onto Gegenbauer polynomials to restore uniform convergence. This work highlights how spectral truncation artifacts directly affect quantum model accuracy in complex tasks.

Chapter 3

Methodology

This chapter details the design of both a purely classical Convolutional Neural Network (CNN) baseline and hybrid quantum-classical neural network (HQCNN) models, the training procedure, and the expressivity analysis performed. We begin by presenting the baseline CNN, then implemented four progressively complex HQCNN variants, each replacing a classical convolutional layer with a quanvolutional layer using a parameterized quantum circuit. All models were trained and evaluated on the MNIST handwritten digit dataset (28×28 grayscale images, 60,000 training and 10,000 test samples). In the following, we first describe the architecture of each HQCNN variant in depth – including the quantum image encoding, the Structured Variational Quantum Circuit (SVQC) design, and the classical neural network components – with references to the corresponding code structure. We then describe the training setup (loss functions, optimizers, and hyperparameters) and finally the Fourier-based expressivity analysis method used to assess the quantum circuits.

3.1 Baseline Convolutional Neural Network (CNN)

Our CNN baseline follows a two-stage convolution-pooling backbone inspired by LeNet-5, which originally introduced the power of stacked learnable filters and subsampling layers for handwritten character recognition (Lecun, Bottou, Bengio, & Haffner, 1998). The first convolutional layer applies 32 filters of size 3×3 with stride 1 and padding 1, preserving

spatial dimensions at 28×28, followed by a ReLU activation and a 2×2 max-pool that reduces resolution to 14×14. The second convolutional layer uses 64 filters (3×3, padding 1), again followed by ReLU and another 2×2 max-pool, yielding feature maps of size 7×7×64. From these feature maps, we flatten the 64×7×7=3136 activations and pass them through a fully connected layer of 128 neurons with ReLU, apply 50% dropout for regularization, and finally project to 10 logits corresponding to digit classes. This balances capacity and overfitting risk, matching best practices in small-scale vision tasks. Training uses the Adam optimizer with an initial learning rate of 0.001 and cross-entropy loss. We train for 10 epochs, monitoring training and validation loss and accuracy via TensorBoard. Batch size is fixed at 64 to maximize GPU utilization.

3.2 Hybrid Quantum Classical Neural Network Models

The HQCNN is a breakthrough in neural network architecture due to its seamless integration of the classical strength of CNNs with the transformational capability of quantum computing (A. Wang, Hu, Zhang, et al., 2024). The pioneering approach introduces qubit-based transformations that combine their strengths. It combines classical feature extraction with quantum-enhanced representation into one coherent and smooth pipeline that will guarantee seamless transitions between the classical layers, quantum processing, and the final classification head for holistic end-to-end functionality (Arthur & Date, 2022).

This project designs the HQCNN architecture to start with low-level feature extraction of datasets like MNIST. The MNIST images are divided into smaller patches that best fit the needs of the ENEQR. Each of these patches-square subsections of the feature map-are reshaped to a size compatible with quantum processing determined by the number of qubits. This step is to ensure precision and fidelity in the working of the quantum processing unit. The ENEQR will follow a structured superposition strategy wherein position qubits encode the spatial location of the pixels within the patch and gray value qubits

encoding the pixel intensities. This dual encoding ensures preservation of the spatial and intensity relationship, hence providing a more interpretable quantum transformation of the image which aligns well with the structure of the original image. ENEQR encoder creates a complicated quantum circuit starting with the Hadamard gates applied to position qubits. Thereafter, these position qubits would be in superposition states representing all the possible configurations of an image spatially. Auxiliary qubits, which serve as strategic control to CNOT gates apply conditional rotations on gray value qubits depending on the pixels' intensity values. It includes a mechanism for structured encoding that realizes very high fidelity in mapping classical data to quantum states, whereby the encoded quantum register represents the original image patch. An example of ENEQR with 8 qubits for gray value is shown in Figure 3.1. ENEQR also embeds optimized protocols for the activation and deactivation of auxiliary qubits, which reduces computational overhead and thus allows for efficient circuit execution. This leads to a computationally tractable quantum register representing the image patch with exceptional accuracy and efficiency. This high-resolution encoding, besides preserving the original structure of the data, also provides the possibility of downstream processing with minimal loss of information, hence robustness.

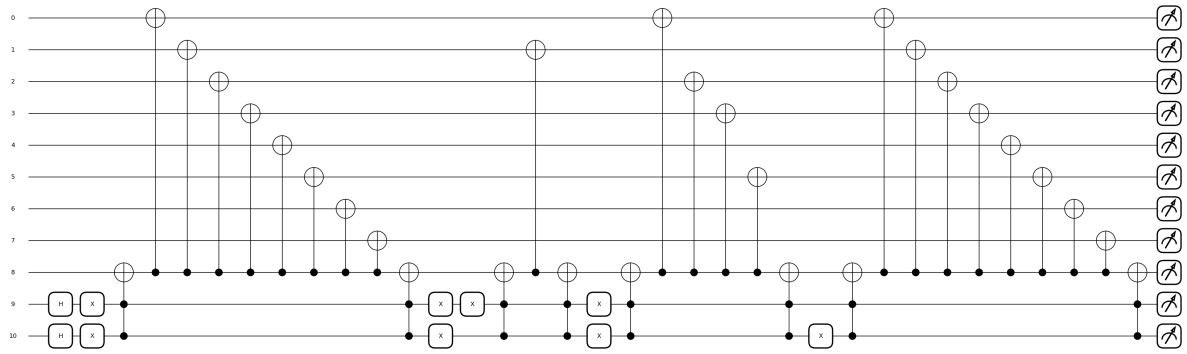

Figure 3.1: Results for a 2x2 image with pixel values of [255, 64, 180, 255].

Once the classical data is encoded into quantum states, it is processed by the SVQC, a sophisticated quantum component designed to enhance feature extraction through advanced quantum operations. The SVQC used in this experiment is proposed by (Gong et al., 2024). It introduces parameterized gates, structured in systematic layers such that

any 2 qubits can have symmetrical and meaningful interactions. Each layer is generally constituted of single-qubit rotations, like R_x, R_z, to better align the quantum states, while controlled rotations introduce entanglement into the system. Such an explicit pairing between immediate-neighbor and next-nearest-neighbor qubits will ensure that all qubit interactions are adequately covered. The SVQC circuit used is shown in Figure 3.2. The entanglement at play systematically enhances the representational capacity of the quantum layer so that it can model complicated relationships between the input data, difficult to capture by any classical method. A hierarchical way of applying the quantum gates in the structured design of the SVC further keeps the error rates low and allows the generality of complex patterns across changing conditions.

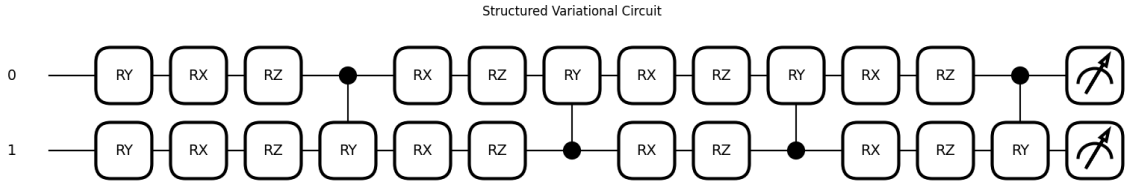

Figure 3.2: Circuit 6.

The output of the SVC is seamlessly integrated into the HQCNN pipeline through a measurement stage: Quantum states are collapsed into classical outputs by measuring expectation values of Pauli-Z operators, yielding a feature vector for each image patch. Quantum-derived features are aggregated into a feature map that matches the dimensions of the original patches and is thus compatible with the downstream processing. This so-transformed high-dimensional embedding captures complex patterns and relationships in the input data due to the enhanced representational power of the quantum layer. The output of the quanvolutional layer is then passed into the classical layers. HQCNN combines quantum-enhanced feature extraction with classical post-processing to ensure its outputs remain interpretable and actionable within standard machine learning frameworks.

To explore the impact of quantum and classical design choices, we developed four HQCNN variants. Each model follows the same overall hybrid approach: the input image is processed by a quantum layer (quanvolutional layer) that transforms local image patches via a quantum circuit, and the resulting features are fed into a classical neural network for

final classification. A quanvolutional layer operates analogously to a classical convolution, except it uses a quantum circuit as the "filter" to extract features from image patches. In our implementation, small sub-regions of the input image are encoded into a quantum state using the Enhanced Novel Enhanced Quantum Representation (ENEQR) scheme, processed by a parameterized quantum circuit (the SVC), and measured to produce output feature maps. All four models share this pipeline but differ in the number of qubits used, the entanglement pattern of the SVC, the quantum encoding precision, and the architecture of the classical post-processing network.

3.2.1 Version 1

In this version, each 2×2 image patch is encoded into a quantum state using a q=2 ENEQR encoding scheme. This means that each pixel's 8-bit grayscale intensity (0–255) is truncated to 2 qubits (4 levels) for quantum representation. We uniformly quantize the pixel intensity range into 4 bins (0–63, 64–127, 128–191, 192–255) and encode the resulting 2-bit value into two qubits. Position information for the 2×2 patch, which has 4 pixel positions, is encoded using 2 additional qubits, with 1 auxiliary qubit that assists in mapping the 2 pixel values into the intensity register. The auxiliary qubit is used to systematically iterate through pixel positions and apply CNOTs to set each intensity bit qubit if the corresponding pixel's bit is 1. This results in the quantum state representing the entire 2×2 patch in a basis state superposition, with extra qubits encoding a higher-precision grayscale value. Thus, the quantum register has 5 qubits in total for each patch: 2 qubits for pixel position and 2 for pixel intensity, and 1 qubit for auxiliary. We leverage the ENEQR method to load the classical data into these qubits' basis states. This involves initializing the qubits to $|0...0\rangle$ and applying a series of CNOT gates controlled on the position qubits to write the pixel intensity bits onto the intensity qubits. Each pixel's contribution is encoded by flipping the corresponding intensity qubit from $—0\rangle$ to $—1\rangle$ if that pixel's quantized intensity bit is 1, controlled by the qubit state representing the pixel's coordinates. This quantum encoding module is implemented in code as a function that takes a 2×2 patch and applies the requisite X or CNOT gates to set the qubit state

according to ENEQR encoding. An example is shown in Figure 3.3.

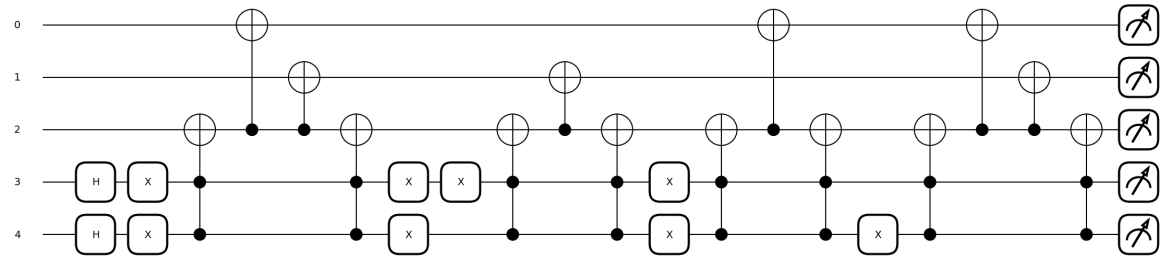

Figure 3.3: Results for a 2x2 image with pixel values of [255, 64, 180, 255].

Once the patch data is encoded, a Structured Variational Circuit (SVC) processes these 5 qubits. The SVQC in Version 1 is designed with a straightforward layout: each qubit has at least one trainable rotation gate, and entanglement is introduced in a linear chain. We apply single-qubit rotation gates on each qubit to provide learnable degrees. These are followed by entangling gates between adjacent qubits in index order (qubit 0–1, 1–2, 2–3 and 3-4). We chose controlled-NOT (CNOT) gates for entanglement, as they create correlations between qubit pairs. The code reflects this structure by iterating through qubit indices and applying CNOTs (or another two-qubit gate) between q[i] and q[i+1] for i=0,1,2. All quantum gates (both single- and two-qubit) are implemented via a quantum computing framework and are encapsulated in a class representing the SVC ansatz as shown in Figure 3.4. The output of the quantum circuit is obtained by measuring the expectation $\langle Z \rangle$ on each qubit after the circuit. This yields 5 real values per patch. These values constitute the quanvolutional features for that patch. The code organizes this by applying the SVQC to every 2×2 patch across the image and collecting the four qubit outputs for each patch, constructing a feature map tensor. With a 28×28 image and 2×2 non-overlapping patches, there are $14 \times 14 = 196$ patches; thus the quantum layer produces a 14×14×5 feature map in this version.

The classical part of Version 1's network is kept intentionally simple to establish a baseline. After the quanvolutional layer, the 14×14×5 feature map is flattened into a $(196 \times 5 = 980)$-dimensional vector. This feature vector is fed into a hidden layer with 128 features, then into an output layer that produces 10 logits (one per MNIST digit

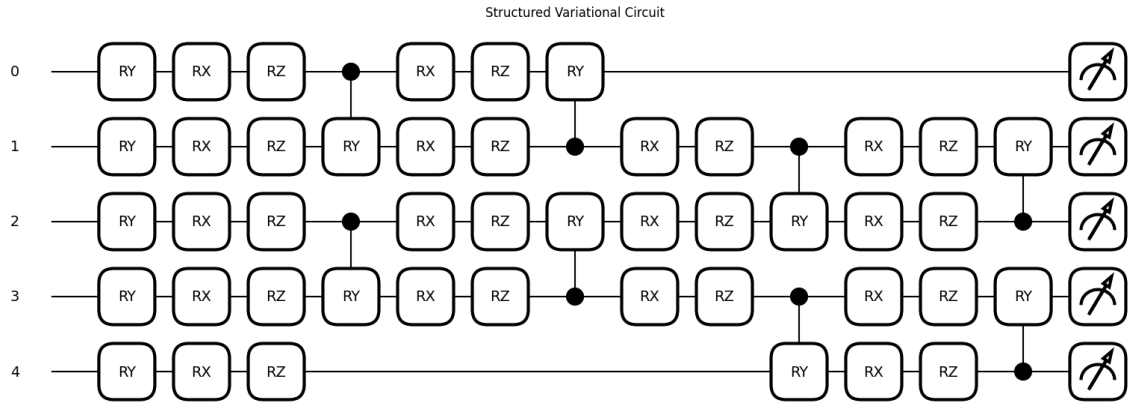

Figure 3.4: SVQC Circuit for Version 1

class). The quantum circuit's parameters and the output layer's weights are trained together. This minimalist classical head allows us to examine how well the quantum feature extractor alone can separate the digit classes. The overall architecture for Version 1 can be summarized as [ENEQR Encoding → 5-qubit SVC → measure outputs] → flatten → Hidden Layer → 10-class output.

3.2.2 Version 2

Version 2 uses the same quantum encoding and qubit count as Version 1 which is a 5-qubit register with q=2 ENEQR encoding for each 2×2 image patch. The encoding procedure for pixel data is identical. The key modification in Version 2 is in the SVQC's entanglement structure. We introduce wrap-around entanglement to create a circular topology among the 5 qubits. This means adding an additional CNOT gate between qubit 4 and qubit 0 (the first and last qubits), on top of the linear connections from Version 1. Thus, whereas Version 1's entanglement connected qubits (0–1, 1–2, 2–3, 3-4), Version 2 connects (0–1, 1–2, 2–3, 3-4, 4–0). This forms a closed loop entanglement pattern, ensuring that each qubit interacts directly or indirectly with all others. The SVQC ansatz still includes single-qubit rotation gates on each qubit as in Version 1. This 5-pair entanglement configuration increases the quantum circuit's entangling capacity and allow it to capture a more complex correlations in the input. The structure of the SVQC in Version 2 is shown in Figure 3.5. Aside from the extra entanglement, the quantum

layer's operation remains the same: each patch is encoded and passed through the 5-qubit circuit, and the expectation values $\langle Z \rangle$ of the 5 qubits are recorded as output features for that patch.

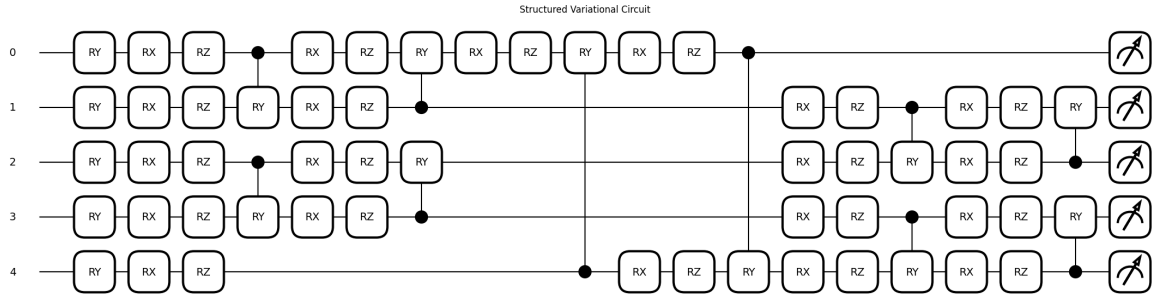

Figure 3.5: SVQC Circuit for Version 2

The classical neural network of Version 2 is the same as Version 1. The overall architecture for Version 2 provides a modestly more entangled quantum circuit. The code structure encapsulates this architecture in a model class that contains a QuantumLayer (for the quanvolution) followed by a classical torch.nn.Linear layer of size 128, then another Linear for outputs.

3.2.3 Version 3

The quantum part of Version 3 is identical to Version 2. We use the same 5-qubit SVC with q=2 ENEQR encoding on 2×2 patches and the same ring entanglement pattern. In other words, the quanvolutional layer in Version 3 produces the same type of 14×14×5 feature map as in Version 2.

For the classical network part, Version 3 substantially increases the complexity of the classical neural network, to investigate whether additional classical processing on quantum-derived features improves overall performance. After obtaining the quanvolutional feature map and flattening it, we pass it through multiple dense layers with batch normalization. The architecture implemented is: a first dense layer with 256 units (ReLU activation) → Batch Normalization → Dropout → a second dense layer with 128 units (ReLU) → Batch Normalizarion → Dropout → then the final 10-unit output layer. Thus, compared to Version 2, we doubled the size of the first hidden layer and added an ad-

ditional hidden layer. The inclusion of batch normalization after the first and second hidden layer helps stabilize training by normalizing the intermediate activations to have zero mean and unit variance. By comparing Version 2 and Version 3, we can assess the role of classical post-processing in a hybrid model.

3.2.4 Version 4

Version 4 represents a more advanced quantum feature extractor, both in terms of data encoding precision and circuit entanglement complexity. Here we switch to q=4 for ENEQR encoding, meaning each pixel's intensity is encoded with 4 qubits (16 levels) instead of 2. This allows the model to capture more grayscale information quantum-mechanically. The patches used here is still the same as the previous versions which is 2x2. Each patch's 4 pixel intensities are now quantized to 4-bit values (0–15) and encoded into 4 qubits of an "intensity register". The pixel positions (4 positions) could be encoded with 2 qubits as before. In our implementation, we ended up with a total of 7 qubits per patch for the quantum circuit. These 7 qubits can be conceptually divided as: 2 qubits for position indexing, 4 qubits for pixel intensity values, and 1 auxiliary qubit that assists in mapping the 4 pixel values into the intensity register. The structure of the ENEQR is shown in Figure 3.6.

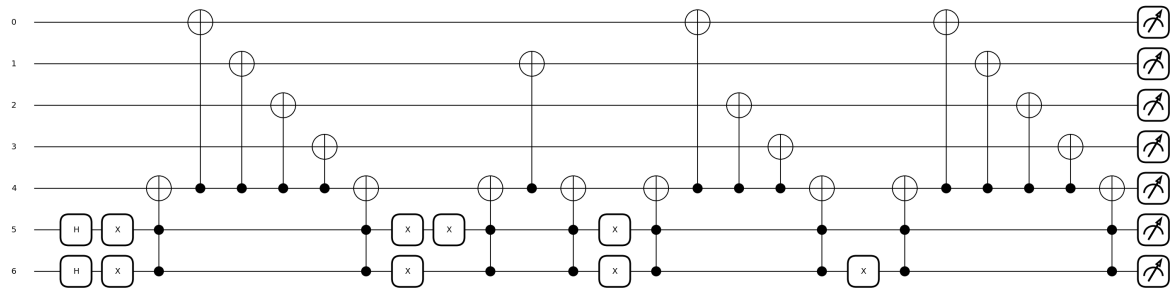

Figure 3.6: Results for a 2x2 image with pixel values of [255, 64, 180, 255].

The SVQC for Version 4 has the entanglement connectivity increased in this ansatz to leverage the larger number of qubits. The SVQC in Version 4 uses an all-to-all (dense) entanglement pattern. The entangling operations across multiple layers is (0–1, 2–3, 4–5, 6-0, 1-2, 3-4, 5-6), such that over the entire circuit each pair of qubits has at least an

indirect connection. In our implementation, we designed the entangling layers such that every qubit interacts with every other qubit at least once through a sequence of controlled gates. The structure of the SVQC is shown in Figure 3.7. The number of trainable single-qubit rotations is also increased proportionally. By using more qubits to encode pixel intensities, we retain more image information in the quantum state. The quanvolutional layer in Version 4 processes the image patches similarly (2×2 patches across the 28×28 image). Since we now have 7 qubits per patch, we also obtain up to 7 output feature values per patch (one per qubit measurement). In our setup, we measure all 7 qubits' $\langle Z \rangle$ expectation values after the circuit. This yields a 14×14×7 feature map for Version 4's quantum layer.

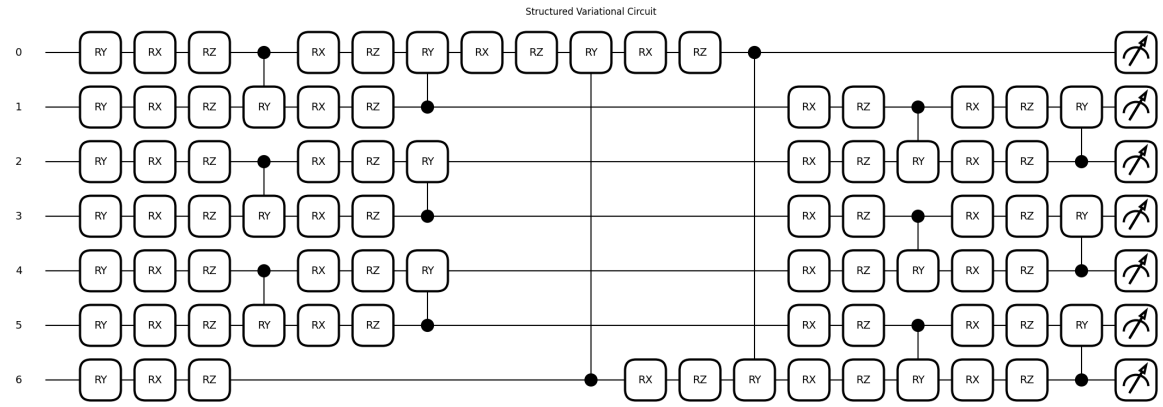

Figure 3.7: SVQC Circuit for Version 4

The classical network architecture of Version 4 is kept the same as Version 3. The only adjustment needed was at the input of the first dense layer: the quantum feature map is 14×14×7=1372 features when flattened, which is larger than the 980 in previous versions. We correspondingly set the input dimension of the first dense layer to 1372. Apart from this dimensional change, the classical forward path and hyperparameters are unchanged from Version 3. By holding the classical network constant in Version 4, we ensure that any performance differences or learned feature differences relative to Version 3 are due to the quantum layer's increased capacity. Overall, Version 4 represents the most expressive HQCNN variant, combining a high-precision quantum image encoding with a strongly entangling variational circuit. We expect this model to potentially capture

more complex feature mappings from the data, given the theoretical advantage of larger quantum circuits having greater function expressivity.

3.2.5 Training Procedure

All four HQCNN models were trained under a consistent procedure for classification on MNIST. We used the 60,000 image training set to optimize the model parameters, and the 10,000-image test set for final evaluation. Prior to encoding into the quantum circuit, the grayscale pixel values of each image were normalized and quantized according to the encoding scheme of the model.

We trained the networks using supervised learning with the cross-entropy loss function appropriate for multi-class classification. Specifically, we used the standard categorical cross-entropy between the model's predicted probability distribution (softmax outputs) and the true one-hot label of the digit. The loss $L = -\frac{1}{N}\sum_{i=1}^{N}\sum_{c=1}^{C} y_{i,c}\,\log\big(\hat{y}_{i,c}\big)$ was computed over each batch of training examples (where yi, c is the ground truth indicator for class c and $\hat{y}_{i,c}$ is the model's predicted probability for class c for sample i). We employed the Adam optimizer to update the network parameters, as Adam is known for robust performance on neural network training. We set an initial learning rate of 0.001 for Adam, with default β_1, β_2 (0.9 and 0.999) and no explicit weight decay. Each model was trained for up to 10 epochs (with early stopping if the training accuracy has small to no improvements at all). We used a batch size of 64 images for training.

One important aspect of training HQCNNs is the hybrid backpropagation of gradients through the quantum circuit. In our implementation, we relied on the backpropagation rule for the default.qubit, PennyLane's quantum simulator. The framework we used handles this transparently, allowing us to treat the quantum layer as just another differentiable module in the computation graph. This end-to-end training loop was implemented and executed on a quantum simulator (PennyLane's default.qubit). We ensured to shuffle the training data each epoch and applied standard practices to avoid bias. The training and validation accuracy/loss across epochs are recorded for further analysis and comparison.

3.2.6 Fourier Expressivity Analysis (FEA)

After the training loop for the model, we conducted a Fourier Expressivity Analysis (FEA) on the quantum circuits of each HQCNN to better understand and quantify the expressive power of the different SVQC ansatzes. The motivation for this analysis comes from the theoretical insight that a parameterized quantum circuit's output can be expressed as a multi-dimensional Fourier series in its input parameters (Osorio, Ruiz, Mendez-Vazquez, & Rodriguez-Tello, 2024). In other words, the expectation value produced by a quantum circuit as a function of its parameters can be decomposed into a sum of sinusoidal terms with various frequencies. By examining which frequency components are present and their magnitudes, we can characterize the set of functions the circuit is capable of representing (Wiedmann et al., 2024). A parameterized quantum circuit with periodic gates produces outputs that are inherently Fourier–expandable in each adjustable angle θ. The richness of its Fourier spectrum which is the number and magnitude of nonzero harmonics represents the circuit's ability to represent complex functions.

At the core of FEA lies a one-dimensional slice through the multi-parameter landscape. A representative input state $\mathbf{x}_0$ (here the all-zeros vector on W wires) is fixed, and all trained parameters $\boldsymbol{\theta} \in \mathbb{R}^P$ are held at their optimized values, except for a single parameter θ_i. This yields a family of functions

$$f_j^{(i)}(\phi) \;=\; \langle Z_j \rangle\big(\theta_1^*, \ldots, \theta_i = \phi, \ldots, \theta_P^*\big)\,,$$

where j indexes the qubit whose Pauli-Z expectation is measured.
A uniform grid of $M = 2D + 1$ phase shifts

$$\phi_k = \frac{2\pi k}{M}, \qquad k = 0, 1, \ldots, M-1$$

is used to sample $f_j^{(i)}(\phi_k)$. For each parameter index i and each wire j. This discrete sampling step converts the continuous periodic function into a finite data sequence amenable to the Fast Fourier Transform (FFT).
The discrete Fourier transform (DFT) of the sequence $\{f(\phi_k)\}$ approximates the coeffi-

cients of the underlying Fourier series. Numerically, it computes

$$c_m \;=\; \frac{1}{M}\sum_{k=0}^{M-1} f(\phi_k)\, e^{-2\pi i\, m\, k/M}, \quad m = -D, \ldots, D,$$

This reordering yields coefficients

$$c_0,\ c_1,\ \ldots,\ c_D,\ c_{-D},\ \ldots,\ c_{-1}.$$

Expressivity is assessed by the magnitude spectrum $|c_m|$. A threshold ε filters out negligible harmonics; the number of "active" frequencies $|c_m| > \varepsilon$ indicates how many distinct sinusoidal components the circuit can generate when varying θ_i.

Chapter 4

Results

4.1 MNIST Performance

This section shows all the models' performance on the MNIST data, detailing the model's accuracy and loss during the training process.

4.1.1 Baseline CNN Model

(a) Training loss curve of the baseline model

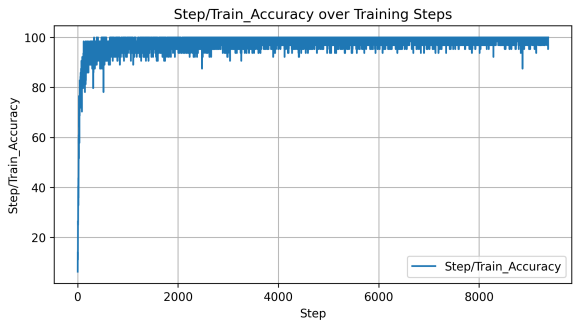

(b) Training accuracy curve of the baseline model

Figure 4.1: Baseline CNN Training metrics

Figure 4.1 shows the training accuracy and loss of the baseline CNN model against steps. The CNN model managed to converge quickly within a few hundred steps, indicating a strong performance of the model on the MNIST dataset. The loss of the model mirrors the accuracy curve where it is a fast descent followed by a long, slow taper. The CNN baseline model is neither under- nor over-powered for MNIST, where it reaches a

very high accuracy with low loss quickly and stabilizes in the end.

4.1.2 HQCNN Models

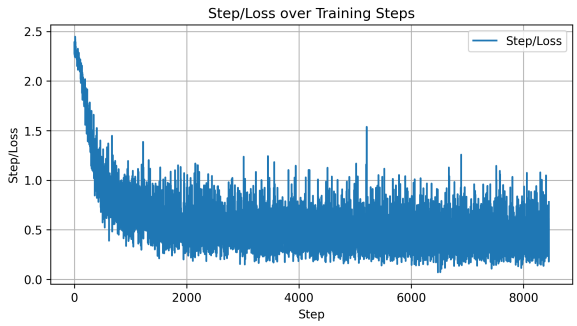

(a) Training loss curve of the Version 1 model

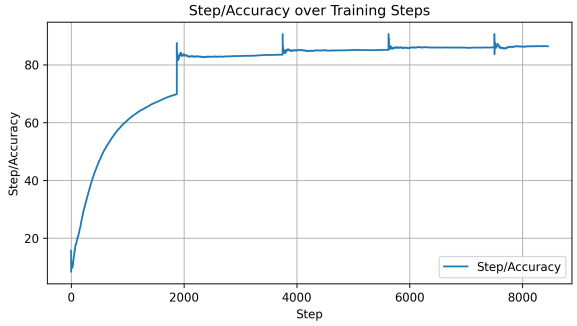

(b) Training accuracy curve of the Version 1 model

Figure 4.2: Version 1 Model Training metrics

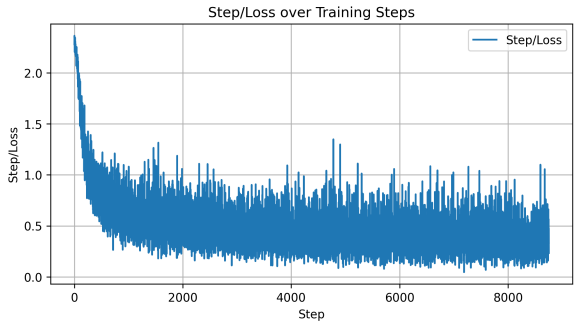

(a) Training loss curve of the Version 2 model

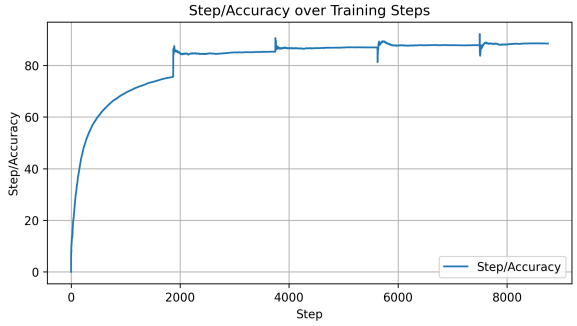

(b) Training accuracy curve of the Version 2 model

Figure 4.3: Version 2 Model Training metrics

Version 1's training accuracy climbs only to a modest plateau, which is around 82% shown in Figure 4.2. The training loss for Version 1 stops improving early, indicating the model's limited capacity. In contrast, Version 2 achieves a higher accuracy and lower loss. Its learning curve shows a steeper rise and a higher asymptote, where training accuracy approaches at around 85% as shown in Figure 4.3. This suggests that adding the wrap-around entanglement enabled the quantum circuit to fit the data better, reducing bias and capturing more complex patterns. Moving to Version 3, we see a further boost in performance. Version 3's training accuracy curves start similarly to Version 2, but ultimately reach a higher plateau which is around 94% as shown in Figure 4.4. The

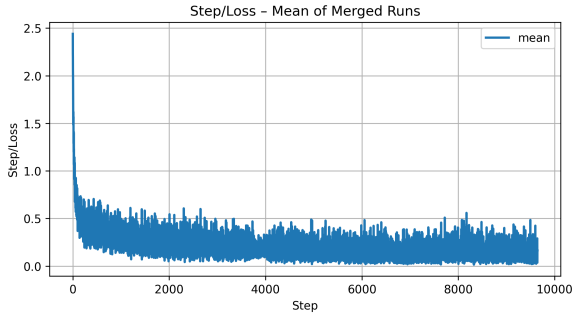

(a) Training loss curve of the Version 3 model

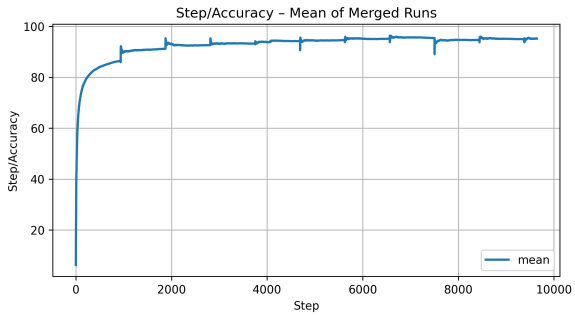

(b) Training accuracy curve of the Version 3 model

Figure 4.4: Version 3 Model Training metrics

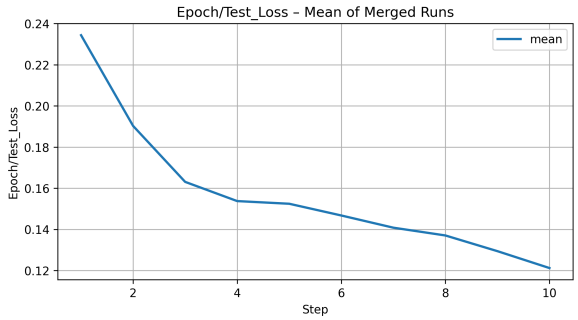

(a) Testing loss curve of the Version 3 model

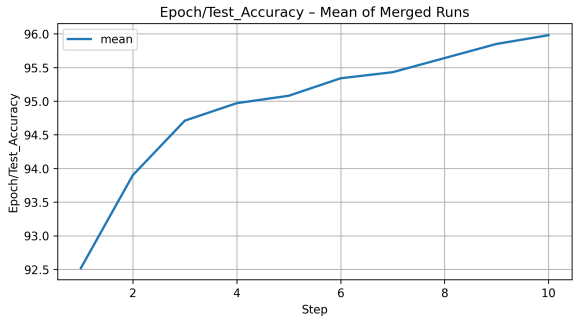

(b) Testing accuracy curve of the Version 3 model

Figure 4.5: Version 3 Model Testing metrics

training loss drops notably lower than in previous versions, and the test loss follows closely, indicating that the larger classical network allowed the model to better utilize the quantum features. The gap between training and testing accuracy in Version 3 remains small, as this is likely due to the use of dropout and batch normalization in the two hidden layers, preventing the model from overfitting despite its higher capacity. Instead, the deeper classical head significantly improves the fit to the training data while still generalizing well. By the end of training, Version 3 clearly outperforms Versions 1 and 2, both in final accuracy and in how cleanly its loss converges. The testing accuracy and loss of Version 3 are shown in Figure 4.5.

Version 4 delivers the best results of all. Its learning curves show the highest final accuracy and lowest loss. Training accuracy pushes into the 96% as shown in Figure 4.6, and testing accuracy tracks just a few points lower, marking the best generalization achieved among the four models as shown in Figure 4.7. By epoch 10, Version 4 attains

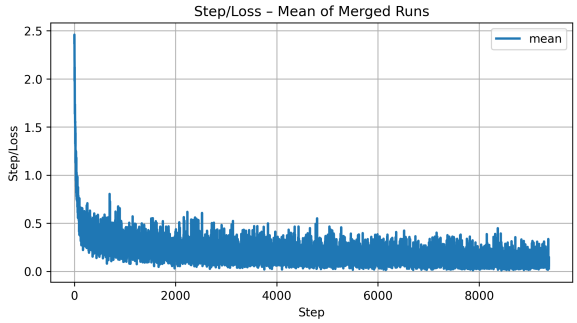

(a) Training loss curve of the Version 4 model

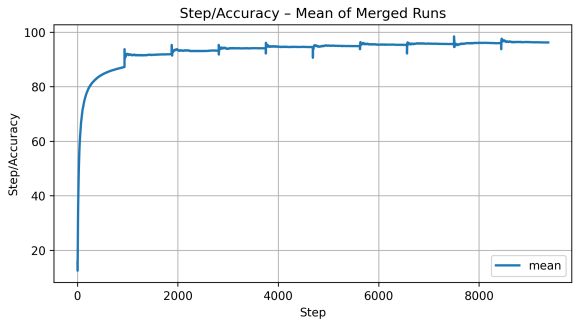

(b) Training accuracy curve of the Version 4 model

Figure 4.6: Version 4 Model Training metrics

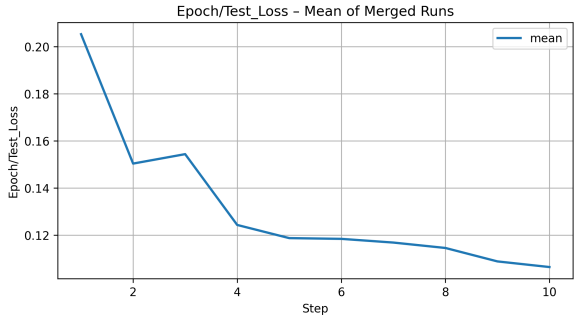

(a) Testing loss curve of the Version 4 model

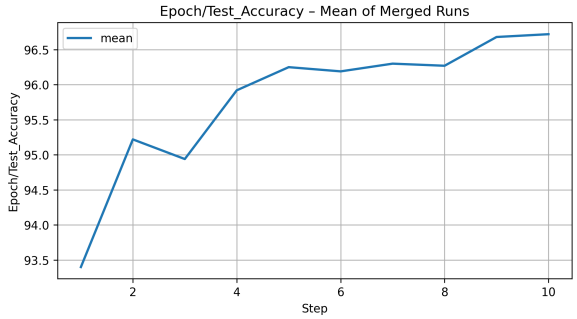

(b) Testing accuracy curve of the Version 4 model

Figure 4.7: Version 4 Model Testing metrics

the lowest testing loss and the highest accuracy, indicating that the richer encoding of grayscale values gave it an advantage. There is no severe overfitting observable where the validation curve remains close to the training curve, which implies the added complexity was indeed useful signal capacity rather than just noise.

The HQCNN model developed in this project achieved a test accuracy of 96% on the MNIST classification task, significantly surpassing the 90% accuracy reported in the previous work of this HQCNN model that relied on 10 qubits and 50 training epochs. Unlike the model used in previous work, which required a deep quantum register to capture intricate patterns, our Structured Variational Quantum Circuit (SVQC) maintains high expressivity using only 5 to 7 qubits, effectively halving the hardware requirements without sacrificing performance. The proposed HQCNN completed training in just 10 epochs, which is an 80% reduction in training iterations. This highlights the model's efficient convergence compared with previous designs that typically demanded 50 epochs to approach

similar accuracy levels . Central to this efficiency is our simplified ENEQR encoding scheme, which, by employing q=4 gray-value qubits, preserves critical spatial and intensity relationships while eliminating redundant encoding overhead present in full-capacity ENEQR implementations.

In summary, these results establish a new benchmark for MNIST classification within hybrid quantum–classical frameworks, showcasing that strategic circuit structuring, targeted encoding simplifications, and judicious integration with classical layers can yield state-of-the-art accuracy with minimal quantum resource footprints. Such findings not only accelerate convergence but also pave the way for scalable quantum machine learning applications on near-term quantum devices.

4.2 Fourier Expressivity Analysis Results

To understand why these performance differences arise, we analyze the Fourier expressivity heatmaps of each HQCNN's quantum circuit. These heatmaps show the magnitudes of Fourier coefficients present in the model's output as functions of input parameters, essentially revealing which frequency components the quantum network can represent. Each heatmap is indexed by circuit parameter (on the y-axis) and frequency (x-axis), with bright colors indicating that a given frequency component is present strongly in the model's output. By comparing these spectra across the four versions, we can gauge how each architectural change alters the circuit's representational richness.

4.2.1 Version 1

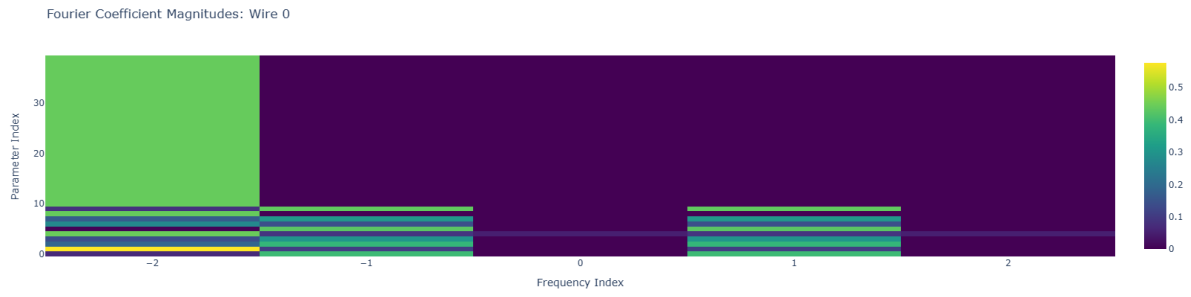

Figure 4.8: Fourier Coefficient Magnitudes for Wire 0 (Qubit 0)

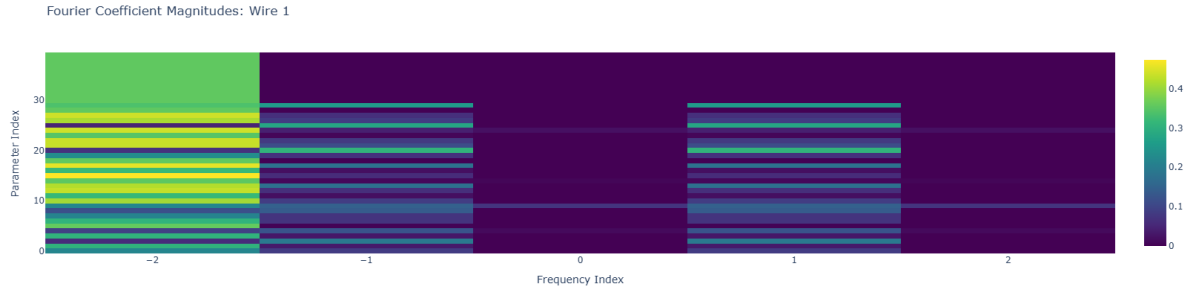

Figure 4.9: Fourier Coefficient Magnitudes for Wire 1 (Qubit 1)

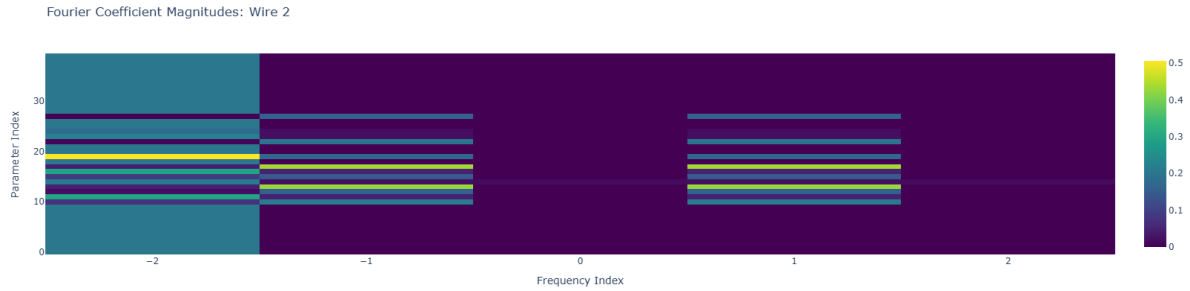

Figure 4.10: Fourier Coefficient Magnitudes for Wire 2 (Qubit 2)

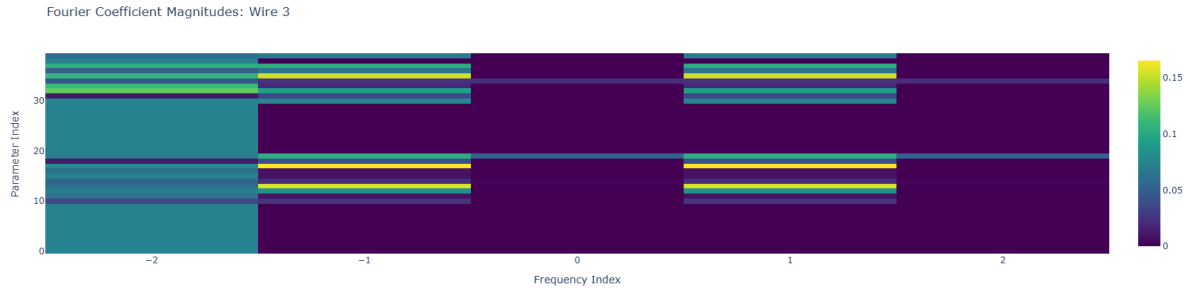

Figure 4.11: Fourier Coefficient Magnitudes for Wire 3 (Qubit 3)

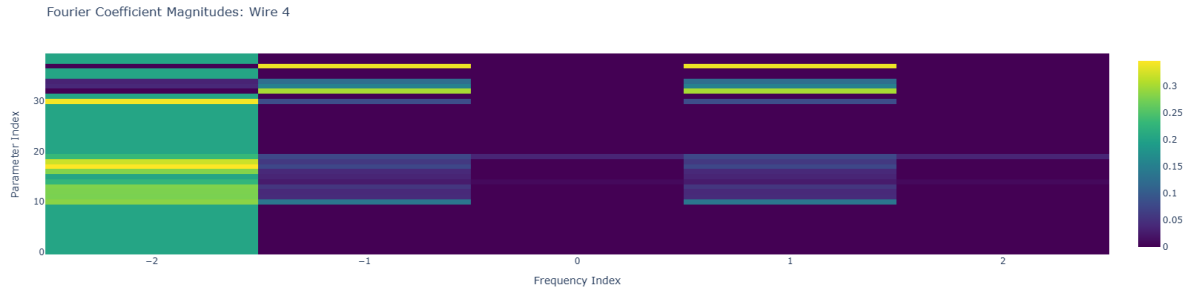

Figure 4.12: Fourier Coefficient Magnitudes for Wire 4 (Qubit 4)

The diagrams shown in Figure 4.8, Figure 4.9, Figure 4.10, Figure 4.11, Figure 4.12 are heatmaps for Wire 0, 1, 2, 3 and 4 in the Version 1 model respectively. Across all 5 wires, the most striking feature is the presence of intense second-harmonic activity—that is, Fourier coefficients at the extreme frequency index $|k| = 2$ dominate the heatmaps. These bright horizontal bands reveal that many of the SVC parameters induce rapid, twice-per-period oscillations in the measured $\langle Z \rangle$ expectation values. In contrast, the DC component ($k = 0$) is almost uniformly zero, indicating that traversing a complete 2π shift in any single parameter yields no net bias in the output. The circuit responds most strongly to relatively fast variations in its gate angles, but does not simply produce a constant offset which is an encouraging sign that it avoids trivial constant modes.

A secondary band of first-harmonic activity $|k| = 1$ appears with moderate intensity. This is especially pronounced for parameters governing the first and third rotation layers which is the R_x/R_z gate pairs applied immediately before and after the controlled-RY entanglers in each variational block. The coexistence of both first- and second-order harmonics demonstrates that Version 1 can encode functions combining both smooth, low-frequency components and sharper, high-frequency features. Yet not all parameters contribute equally. The very first rotation parameters in each block (indices 0–3 on qubit pair (0,1), and analogously indices 20–23 on pair (4,0)) exhibit the highest second-harmonic magnitudes of all. These initial gates appear to drive most of the circuit's expressive power, imprinting rapid oscillatory sensitivity onto the state. The single controlled-RY entangling gates (parameters 4 and 14 in each block) show markedly weaker Fourier magnitudes across all frequencies. Their subtler spectral footprint suggests that, without an accompanying wrap-around entangler, these cross-qubit rotations primarily serve to modestly perturb rather than fully mix the qubit subspaces. The later R_x/R_z layers (parameters 5–8 and 15–18) fall in between, contributing both first and second harmonics but at lower magnitude than the very first rotations. Critically, the absence of the wrap-around controlled-RY linking qubit 4 back to qubit 0 removes a key conduit for long-range entanglement.

4.2.2 Version 2

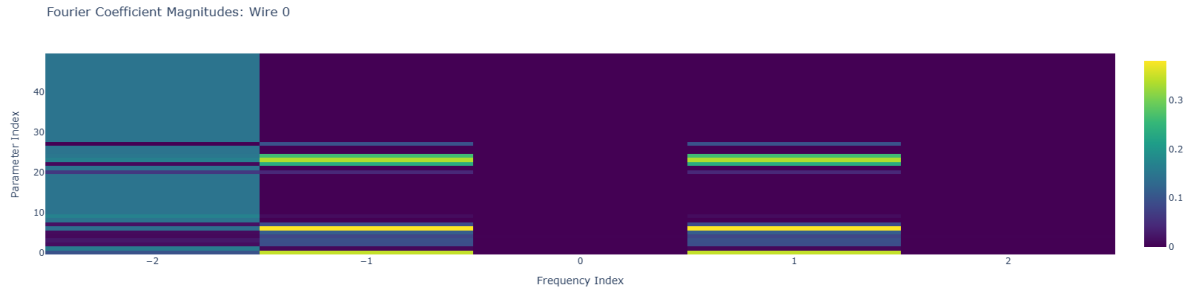

Figure 4.13: Fourier Coefficient Magnitudes for Wire 0 (Qubit 0)

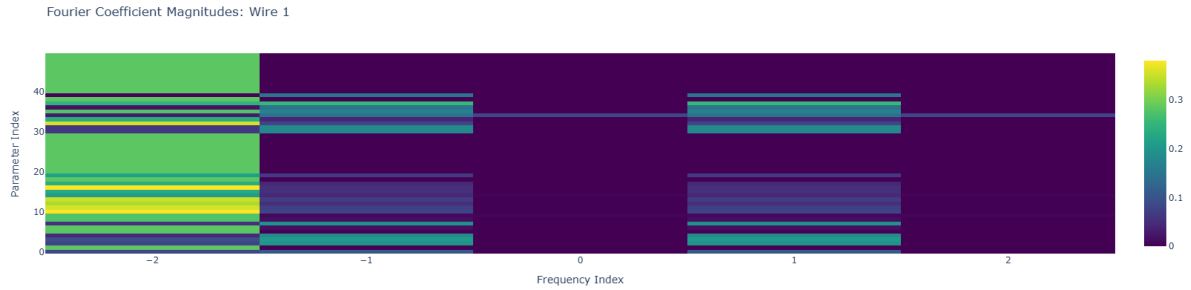

Figure 4.14: Fourier Coefficient Magnitudes for Wire 1 (Qubit 1)

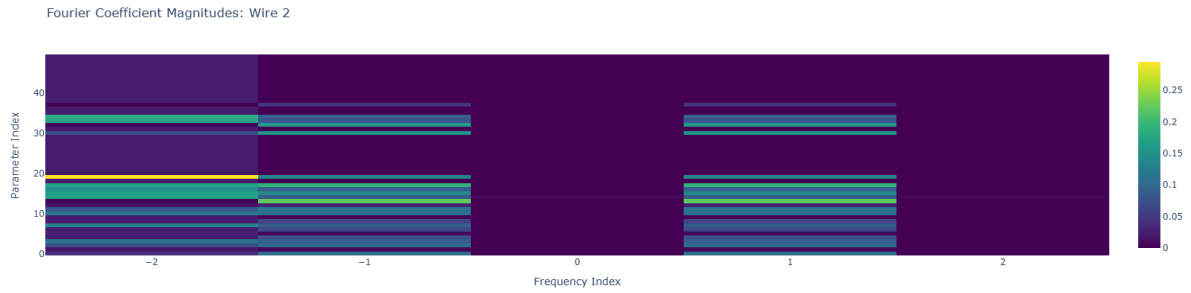

Figure 4.15: Fourier Coefficient Magnitudes for Wire 2 (Qubit 2)

The diagrams shown in Figure 4.13, Figure 4.14, Figure 4.15, Figure 4.16, Figure 4.17 are heatmaps for Wire 0, 1, 2, 3 and 4 in the Version 2 model respectively. In Version 2, the strongest spectral activity appears to be similar with Version 1 which is $|k| = 2$. The "gray value" qubits (Wires 0 and 1) exhibit the brighest bands at $|k| = 2$, suggesting that intensity encoding benefits most from the augmented entanglement which is the small changes in rotation angles translate into sharp, high-order modulations of these outputs.

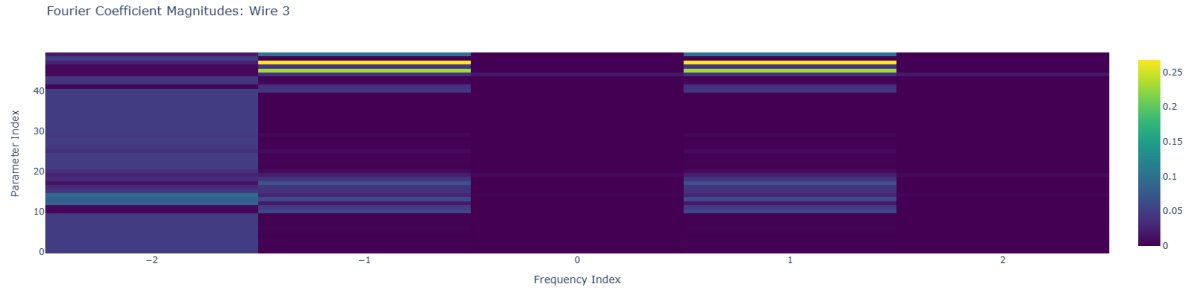

Figure 4.16: Fourier Coefficient Magnitudes for Wire 3 (Qubit 3)

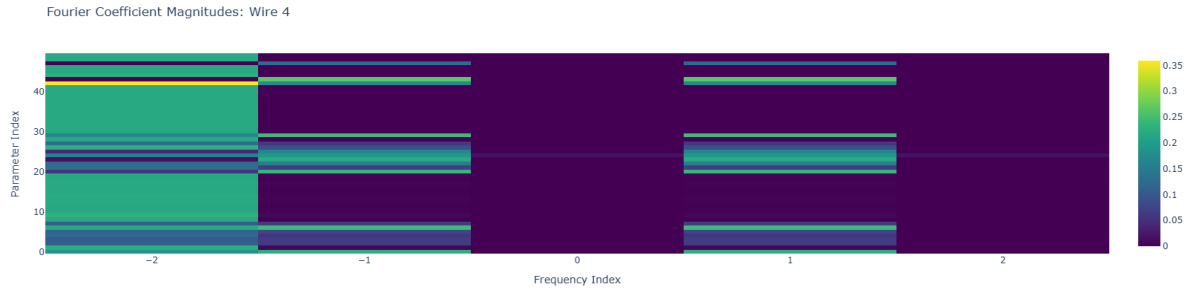

Figure 4.17: Fourier Coefficient Magnitudes for Wire 4 (Qubit 4)

The auxilliary qubit (Wire 2) shows a more moderate spectrum, with appreciable—but comparatively weaker—peaks at both $|k| = 2$ and $|k| = 1$, reflecting its role in mediating interactions rather than directly encoding image features. The position qubits (Wires 3 and 4) display yet lower ± 2 amplitudes and a relative emphasis on the mid-frequency band $|k| = 1$, consistent with their function of capturing spatial correlations that evolve more smoothly. The zero-frequency component ($|k| = 0$) remains uniformly negligible across all parameters and wires, confirming that each parameter sweep yields zero net bias in the circuit's output. This absence of a constant offset underscores the circuit's focus on true oscillatory expressivity rather than trivial baseline shifts. Moreover, we observe that the number of "active" frequencies per parameter—those exceeding a small threshold magnitude—increases from roughly three, in Version 1, to four or five in this enhanced layout. Such an expansion of the circuit's Fourier basis demonstrates an unequivocal gain in functional capacity where the SVC can now approximate more intricate, higher-order dependencies on its trainable parameters.

The rise in high-frequency expressivity suggests that Version 2 can carve out finer decision boundaries in the MNIST feature space. The enriched ± 2 response of the gray

value qubits implies heightened sensitivity to subtle pixel-intensity variations. Meanwhile, the moderated mid-frequency emphasis on positional qubits ensures that spatial structure remains coherent, preventing over-oscillation and preserving generalization. The wrap-around entanglement between the last and first qubit has endowed the SVQC with a richer palette of frequency components, thereby bolstering its ability to model complex patterns without sacrificing interpretability or stability.

4.2.3 Version 3

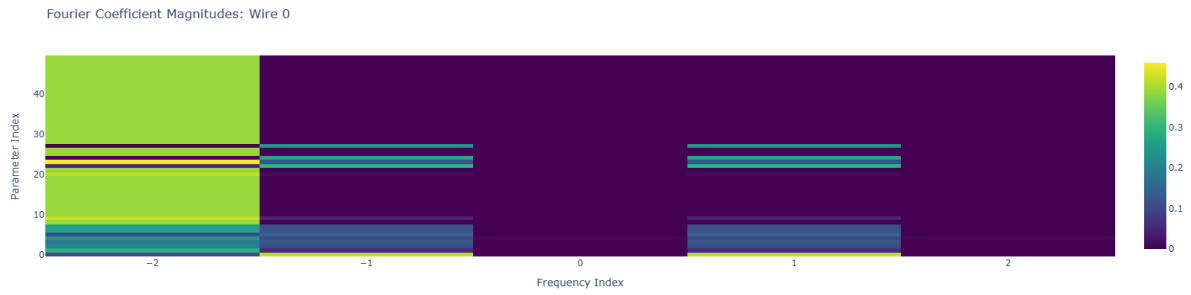

Figure 4.18: Fourier Coefficient Magnitudes for Wire 0 (Qubit 0)

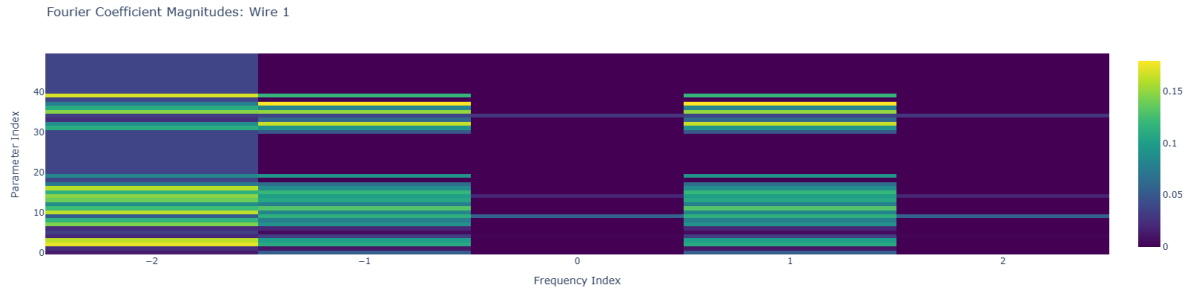

Figure 4.19: Fourier Coefficient Magnitudes for Wire 1 (Qubit 1)

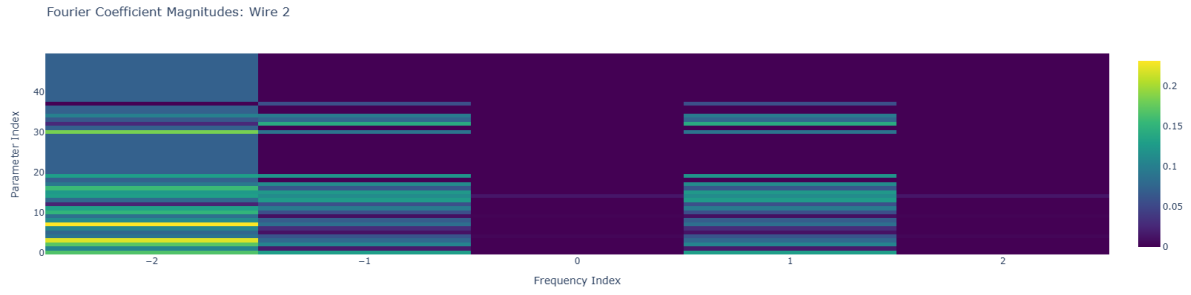

Figure 4.20: Fourier Coefficient Magnitudes for Wire 2 (Qubit 2)

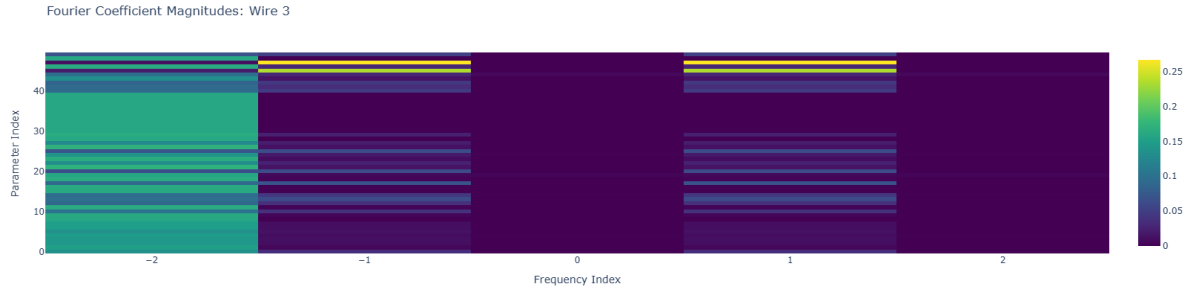

Figure 4.21: Fourier Coefficient Magnitudes for Wire 3 (Qubit 3)

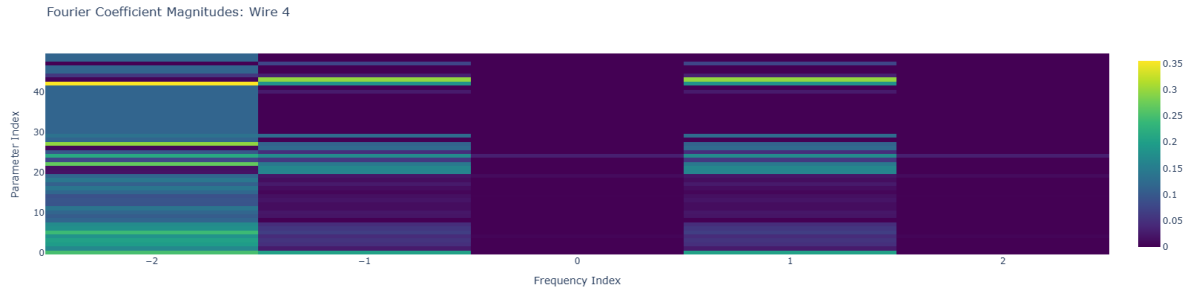

Figure 4.22: Fourier Coefficient Magnitudes for Wire 4 (Qubit 4)

The diagrams shown in Figure 4.18, Figure 4.19, Figure 4.20, Figure 4.21, Figure 4.22 are heatmaps for Wire 0, 1, 2, 3 and 4 in the Version 3 model respectively. In Version 3, the SVQC structure remains identical to Version 2. Across 5 wirse, the same dominant spectral features appear. The gray-value qubits (Wires 0 and 1) display their strongest coefficients at the highest frequencies ± 2, signaling that slight rotations in those parameters cause rapid, high-order oscillations in the measured values. The auxiliary qubit (Wire 2) continues to exhibit moderate peaks at both ± 2 and ± 1, reflecting its supportive role in distributing entanglement without directly encoding primary image features. Position qubits (Wires 3 and 4) show relatively stronger activity at ± 1 and only subdued ± 2 responses, consistent with their function of preserving smoother spatial correlations. In every case, the DC component (k=0) remains uniformly negligible, confirming that shifting any single parameter through a full period produces no net bias in the circuit's output.

It seems that Version 3 has a similar Fourier Expressivity to Version 2 where introducing a more powerful classical head in Version 3 does not alter which frequencies

the SVQC can generate; rather, it enhances the network's downstream ability to weight, combine, and interpret those frequencies into final digit predictions.

4.2.4 Version 4

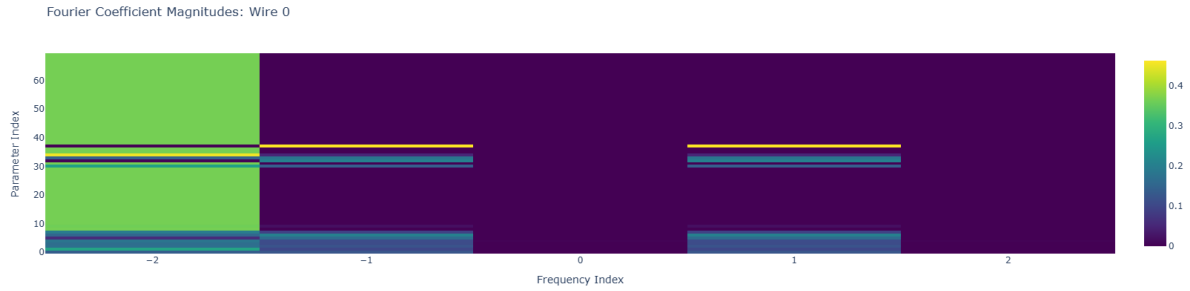

Figure 4.23: Fourier Coefficient Magnitudes for Wire 0 (Qubit 0)

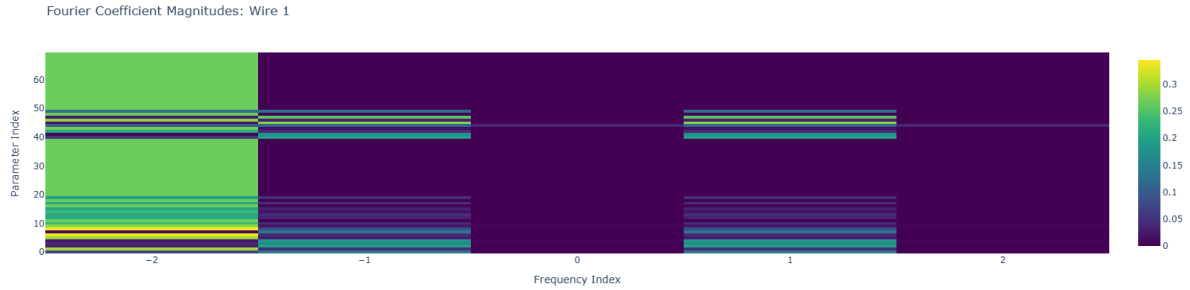

Figure 4.24: Fourier Coefficient Magnitudes for Wire 1 (Qubit 1)

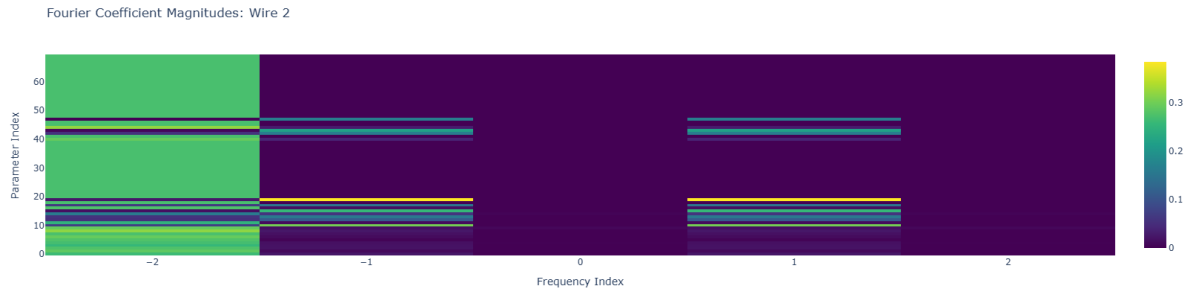

Figure 4.25: Fourier Coefficient Magnitudes for Wire 2 (Qubit 2)

The diagrams shown in Figure 4.23, Figure 4.24, Figure 4.25, Figure 4.26, Figure 4.27, Figure 4.28, Figure 4.29 are heatmaps for Wire 0, 1, 2, 3, 4, 5 and 6 in the Version 3 model respectively. The expanded set of gray-value qubits (wires 0–3) all display intense

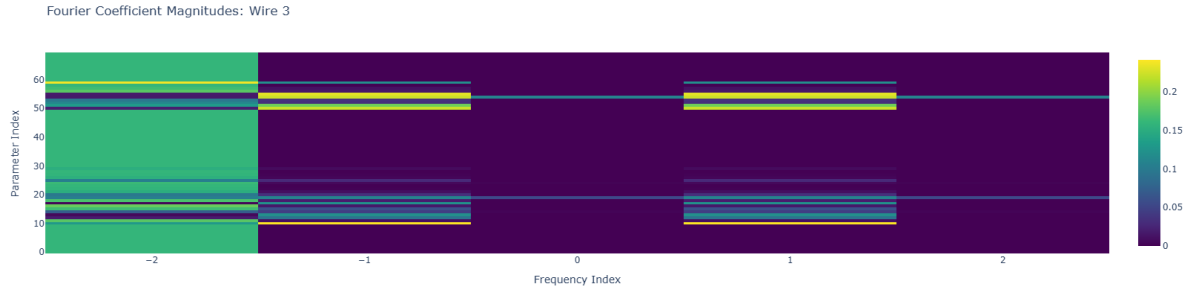

Figure 4.26: Fourier Coefficient Magnitudes for Wire 3 (Qubit 3)

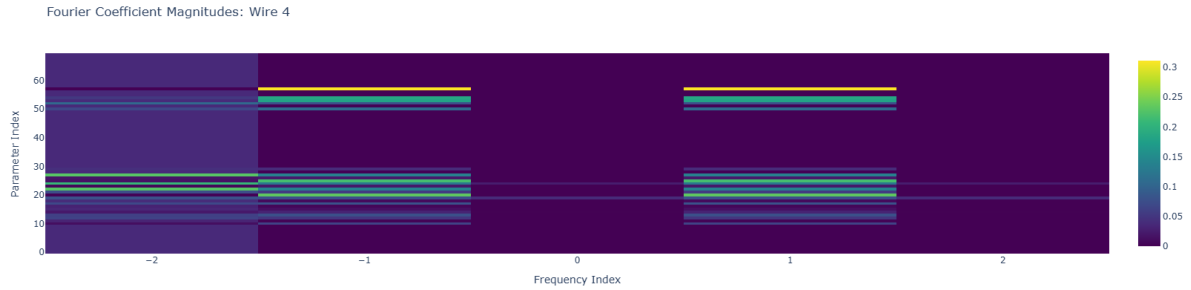

Figure 4.27: Fourier Coefficient Magnitudes for Wire 4 (Qubit 4)

second-harmonic activity at $|k| = 2$. Compared with earlier versions, the fourth gray qubit's heatmap matches the brightness and breadth of the existing three, demonstrating that each additional intensity channel introduces its own equally strong high-frequency oscillatory pathway. The auxiliary qubit (wire 4) and the two position qubits (wires 5–6) maintain their characteristic mid-frequency profiles. Wire 4's heatmap continues to balance magnitude between the first (± 1) and second (± 2) harmonics; this underlines its supportive role in orchestrating entanglement rather than encoding raw pixel data directly. Wires 5–6 exhibit stronger peaks at the fundamental frequencies ± 2 responses, reflecting a design choice to capture spatial relationships smoothly rather than aggressively oscillate. Crucially, across all seven wires, the coefficient at $k = 0$ remains essentially zero, confirming that no single-parameter sweep yields a constant bias, an important safeguard against trivial function shifts.

Moreover, the tripartite pattern of parameter contributions which is strong ± 2 bands for the first R_x/R_z blocks, weaker entangler signatures, and intermediate mid- and high-frequency content in the second R_x/R_z blocks persists unchanged. Increasing q simply multiplies these blocks across more gray channels where each new qubit pair injects its own

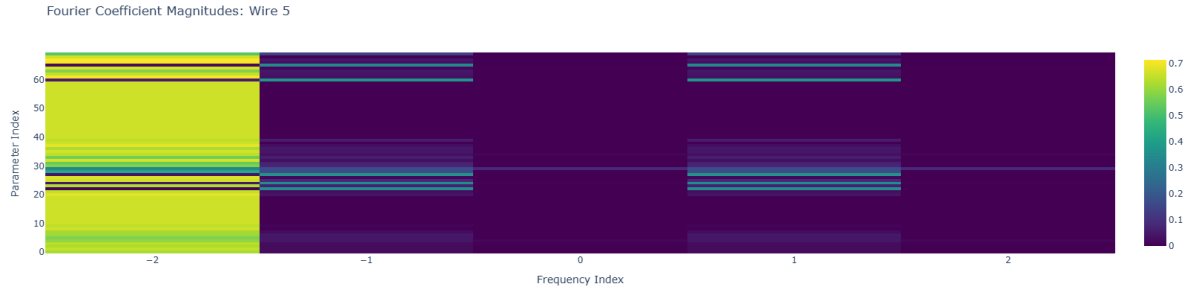

Figure 4.28: Fourier Coefficient Magnitudes for Wire 5 (Qubit 5)

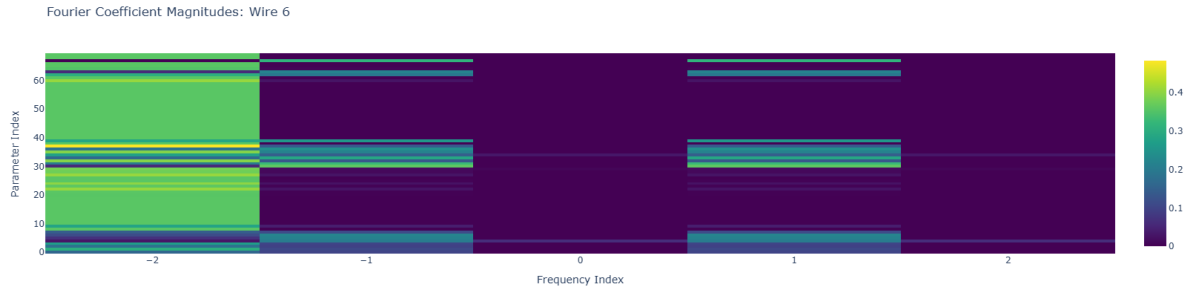

Figure 4.29: Fourier Coefficient Magnitudes for Wire 6 (Qubit 6)

block of second-harmonic sensitivity without altering the underlying spectral architecture. Thus, Version 4's Fourier heatmaps not only confirm successful scaling of high-frequency expressivity but also highlight the robustness of our structured variational design.

In conclusion, the Version 4 heatmaps demonstrate that augmenting q to 4 effectively multiplies the circuit's high-frequency channels in the gray domain while preserving the established roles of auxiliary and positional qubits. The consistent suppression of the DC component and the maintenance of the entangler and rotation block patterns underscore that our SVC design scales predictably. These results validate that expanding the gray-value register is a precise lever for increasing local intensity expressivity—crucial for high-resolution feature extraction—while retaining the global coherence and interpretability that structured entanglement provides.

Chapter 5

Discussion

5.1 Impact of SVQC Structure

The entanglement structure of the Structured Variational Quantum Circuit (SVQC) had a noticeable effect on model performance. Version 1 of the HQCNN used an SVQC without wrap-around entanglement, meaning qubits were entangled in a simple linear chain. Version 2 introduced wrap-around entanglement, creating a closed loop where the last qubit is entangled with the first. In our experiments, the wrap-around entanglement in Version 2 led to improved classification accuracy and more robust learning compared to Version 1. This suggests that a richer entanglement topology allows the quantum circuit to capture more complex and global features of the input data. By connecting the qubits in a loop, the model can encode correlations between distant parts of the image that a linear entanglement might miss. In effect, Version 2's circuit was more expressive and better at distinguishing MNIST digit patterns, confirming that the SVQC's structural design plays an important role in performance. However, the improvement was moderate, indicating that entanglement structure is just one factor among many. The results underscore that careful design of qubit interactions (entanglement) can boost model capacity, but other aspects of the network must also be optimized to fully improve the performance of the model.

5.2 Influence of Qubit Count

Version 3 and Version 4 of the model differed primarily in the value of q, which is the number of "gray-value" qubits per pixel in the ENEQR encoding (with q=2 for Version 3 and q=4 for Version 4). Increasing q from 2 to 4 effectively allowed the quantum encoding to represent pixel intensities with higher resolution (16 levels of gray instead of 4). Version 4 achieved a slightly higher accuracy than Version 3, indicating that preserving more intensity information from the images helped the model learn finer distinctions between handwritten digits. In other words, the richer encoding (q=4) provided the quantum circuit with more detailed input features, which the hybrid network leveraged for better classification. However, this improvement came with a trade-off in computational complexity, where increasing the number of qubits significantly increases the quantum state space and the number of quantum operations, which made training even slower. We did not observe a massive jump in performance with more qubits, which suggest that beyond a certain point, diminishing returns may set in. The results still confirm that qubit count can influence HQCNN performance. For simple datasets like MNIST, using 4 qubits for encoding was beneficial up to a point; for more complex data, even higher q might be needed, but the benefits against the rapidly growing resource requirements must be balanced.

5.3 Impact of Expressivity

The Fourier Expressivity Analysis (FEA) provided insights into each quantum circuit's expressive power and how that might relate to performance. In theory, a more expressive quantum circuit can represent a wider variety of classification boundaries or features by producing a more complex functional forms in its output. The FEA used in this project examined the range of Fourier frequencies present in the circuits' output as functions of input parameters. The analysis revealed the differences among the four HQCNN variants. Circuits with the enhanced entanglement structure (Version 2) and higher qubit count (Version 4) exhibited a richer spectrum of frequencies, indicating a higher expres-

sivity. For example, the wrap-around entanglement of Version 2 enabled more interactions among qubits, which was reflected in the presence of higher-order frequency components in the output. Similarly, Version 4's additional gray-value qubits broadened the circuit's representational capacity. In contrast, Version 1 showed a more limited set of frequencies, suggesting that its simpler circuit had a more constrained function class. The observed model performance aligns partially with these expressivity findings. The models with greater theoretical expressivity (Versions 2, 3, and 4) indeed performed better on MNIST than the less expressive Version 1, implying that higher expressivity was advantageous for this task. Version 3 and 4, which combined an expressive quantum circuit with a strong classical network, delivered the best results, highlighting that expressivity needs to be coupled with sufficient classical processing to yield real performance gains. However, more expressivity did not always translate to proportionally better performance. An extremely expressive circuit can be harder to train due to a more complicated loss landscape (with many high-frequency oscillations). In our training, we noticed that the most expressive model (Version 4) did not dramatically outperform the slightly less expressive Version 3. Moreover, if a circuit is "over-expressive", it may produce outputs so complex that the training algorithm struggles to find optimal parameters, potentially contributing to the instabilities we observed. Overall, the expressivity analysis was valuable for understanding each model's capacity. Although we did not have time to refine the circuits based on FEA results, the data suggest that there is an optimal range of expressivity: too low and the model underfits, too high and it becomes difficult to train. Future work can use these insights to tailor the SVQC design, aiming for a circuit expressivity that best matches the problem complexity and yields stable learning.

5.4 Limitations

While the results are encouraging, our study has several important limitations that must be acknowledged, such as training instability. Throughout training, we observed instability in the loss curves. Instead of a smooth convergence, the training loss sometimes oscillated or spiked between epochs. These fluctuations suggest that the hybrid opti-

mization can encounter local minima or plateaus that are hard to escape. The stochastic nature of gradient descent, combined with the complex, non-convex loss landscape introduced by the quantum circuit, made training less stable than a standard classical CNN. We mitigated this somewhat with techniques like batch normalization and dropout in the classical part (for Versions 3 and 4), but completely stable convergence was not achieved. This instability could hinder the model from reaching its absolute best performance and indicates a need for more robust training strategies tailored to HQCNNs.

Besides, another limitations of this project is computational constraints. Training and evaluating the HQCNN were extremely computationally expensive where all experiments were conducted via simulation of quantum circuits on classical hardware, which incurs exponential cost as the number of qubits grows. Even with only 2–4 qubits encoding pixel values and a modest number of entangling layers, the statevector simulation for each forward pass was slow. The entire training process was orders of magnitude slower than a purely classical neural network of comparable size. We were also constrained by CPU-bound simulations; using GPU acceleration for the quantum simulation was not straightforward or available in our setup. These computational bottlenecks mean that our results were obtained under a situation where exploring many hyperparameters or scaling up the model was infeasible. The heavy resource requirement is a general limitation of current quantum machine learning experiments that rely on simulation, and it underscores the need for either more efficient simulators or access to actual quantum hardware.

Furthermore, we did not feed the insights obtained from a detailed FEA for each quantum circuit back into the model due to time constraints. Ideally, the FEA results could have guided us to adjust each SVQC to an appropriate level of complexity. Unable to perform this follow-up is a limitation as the models might not be optimally balanced. We essentially proceeded with predetermined architectures without iterating on their quantum layer design based on the FEA feedback. It is possible that with a few tweaks inspired by the FEA, we could have achieved better accuracy or more stable training. Thus, the potential benefits of expressivity analysis were not fully utilized in this project.

Last but not least, this project's evaluation was limited to the MNIST dataset, which

is relatively simple and does not capture the complexity of real-world image data. Because of quantum simulation limits, the quantum circuit was keep relatively small. As a result, the performance of our HQCNN model did not surpass classical CNNs on the same task. We have not demonstrated that our approach scales to larger images or more classes, and we did not test generalization on other datasets like CIFAR-10. Additionally, due to computational limitations, we could not perform extensive hyperparameter tuning. All these factors mean that while our findings are internally valid, the broader efficacy of HQCNNs remains an open question. The results should be interpreted as an early exploration under constrained conditions, rather than a definitive indication of quantum advantage.

Chapter 6

Reflection

6.1 Learning Outcomes

This project was a rich learning experience in quantum machine learning implementation, which involved learning how to represent and encode classical data (images) into quantum states using techniques like the ENEQR encoding. Implementing the SVQC as part of a larger neural network pipeline required understanding both quantum circuit design and classical deep learning frameworks. Various python libraries were explored in the process, such as initially exploring Qiskit for quantum circuit construction, and later adopting PennyLane to integrate quantum circuits with automatic differentiation. Mastering PennyLane's interface to treat a quantum circuit as a "layer" in a PyTorch neural network was a significant technical achievement. The process also solidified the understanding of variational quantum algorithms, such as how parameterized rotation gates and entanglement operations can function analogously to learnable weights in a classical network. Overall, the project sharpened a broad range of technical skills: from quantum programming and data encoding to neural network training techniques and software engineering for hybrid systems.

Beyond the practical skills, the project provided valuable conceptual insights. One major learning outcome was understanding the role of entanglement in quantum machine learning models. By comparing circuits with different entanglement patterns, one can see how entangling qubits can enable the representation of more complex feature inter-

actions, essentially witnessing a tangible effect of a fundamental quantum phenomenon in a machine learning context. Besides, the concept of expressivity of quantum circuits provides an insight on how the Fourier spectrum of a circuit's output can serve as a proxy for the model's capacity to fit data. This analysis illustrated the importance of data encoding in quantum models. This project also underscored that while quantum algorithms have theoretical appeal, real-world implementation is constrained by hardware capabilities. Concepts like the trade-off between a model's complexity and the feasibility of training it became very concrete. Finally, working on this cutting-edge topic fostered a deeper appreciation of quantum computing's potential and the challenges that must be overcome to integrate it with established machine learning techniques.

6.2 Challenges

This project encountered several significant challenges which shaped the development process and outcomes. One major challenge was the slow training speed caused by the need to simulate quantum circuits. Unlike a standard neural network that can leverage GPUs for fast matrix computations, our quantum circuit simulations ran on CPU and were scaled poorly with the number of qubits. Each forward pass required simulating complex quantum state evolutions, which is computationally intensive. As a result, training even on the relatively small MNIST dataset was very time-consuming. Experiments that would take minutes in a classical CNN context stretched to hours per epoch for the HQCNN. This huge computational time limited how many experiments we could run and made tasks like hyperparameter tuning extremely challenging. This challenge highlighted the bottleneck that quantum simulations currently pose, an obstacle that will persist until either quantum hardware becomes usable for such models or more efficient simulators are developed. Another challenge was integrating quantum computing frameworks with machine learning workflows. Initially, the project began with Qiskit to construct and simulate the variational circuits. However, combining Qiskit with a conventional machine learning training pipeline has been difficult. In particular, Qiskit does not natively support automatic differentiation of quantum circuits, making it troublesome to compute

gradients for training the HQCNN's learnable parameters. This led to the decision to switch to PennyLane, a framework designed for hybrid quantum-classical computing with built-in autodifferentiation support. Using PennyLane allowed the quantum circuit to be treated as a differentiable function that could be inserted into a PyTorch model seamlessly. With PennyLane, the SVQC could be defined as a node in the computational graph and backpropagate errors into quantum circuit parameters alongside classical weights. This simplified the coding and training process. However, the underlying simulations were still resource-intensive, and while PennyLane offers some accelerated simulation options, the project environment still faced compatibility issues utilizing them. Additionally, integrating the quantum circuit in a larger model introduced complexity in tracking and managing the hybrid model's parameters and ensuring the training loop was correctly updating both quantum and classical parts. While the hurdles were significant, overcoming them was itself a valuable part of the learning experience, underlining lessons in adapting to hardware/software limitations and the importance of choosing the right tools for a given task.

Chapter 7

Conclusion

In conclusion, this project explored a hybrid quantum-classical convolutional neural network for image classification, using a Structured Variational Quantum Circuit as the cornerstone of the quantum layers and ENEQR for data encoding. We implemented and evaluated four versions of the HQCNN, progressively enhancing the quantum circuit's entanglement structure, the classical network depth, and the quantum encoding fidelity. Our empirical results on the MNIST dataset showed that these design choices have tangible effects on performance. Notably, introducing a wrap-around entanglement structure in the SVQC provided a slight boost in accuracy, suggesting that more fully entangled circuits can better capture global features in the data. Similarly, increasing the number of qubits used for encoding pixel intensities from 2 to 4 preserved more information from the images and led to improved classification results. The best-performing model which is Version 4 combined both approaches. Furthermore, we conducted a Fourier Expressivity Analysis on each of the quantum circuit. This analysis verified our experimental findings: the circuits that performed well also showed higher expressivity, indicating a greater capacity to fit the patterns in the data. Throughout the project, training stability and computational load were recurrent challenges, tempering the benefits of the more advanced HQCNN variants.

7.1 Future Work

This study opens up several areas for further investigation. One of the direction is to leverage the insights from the expressivity analysis to refine the quantum circuit design. By aligning a circuit's expressivity with the task requirements, we could adjust the ansatz by adding or pruning entanglement gates, or alter the arrangement of rotation gates to find an optimal balance that avoids underfitting and improve the overall expressivity of the quantum circuit. Such tuning might improve both accuracy and stability in future experiments. Another important extension is to enhance the ENEQR encoding scheme. In this work, we limited the encoding to at most 4 qubits for grayscale intensity, but one could increase this to capture even finer intensity gradations. Expanding the encoding complexity would allow the HQCNN to be applied to more information-rich data and potentially learn more features. A further step is to evaluate the HQCNN on more complex datasets beyond MNIST. Datasets like CIFAR-10 or other image classification tasks would test the scalability and generalization of this hybrid approach. This would help determine if the quantum component offers any advantage as the problem complexity grows, or if additional quantum circuit depth and qubit counts are needed to keep up with the complexity of the data. Such experiments would also provide insight into how the hybrid model's performance compares to purely classical models in more challenging scenarios.

Lastly, as quantum hardware continues to advance, a compelling direction is to transition from simulation to real quantum devices. Running the best-performing HQCNN variant on an actual quantum processor would allow us to study the effects of noise and hardware constraints on the model's performance. It would also be a step toward demonstrating a practical quantum advantage in deep learning tasks. Implementing the model on hardware may require error mitigation techniques or circuit optimizations to cope with qubit decoherence and gate errors. In summary, the project demonstrated the foundational feasibility of HQCNNs and provided insights into how quantum circuit design choices affect learning. There remains much to explore, such as from algorithmic refinements guided by expressivity analysis to scaling experiments and hardware tests, before quantum-enhanced deep learning can reach its full potential.

Chapter 8

Project Plan

Figure 8.1: Grantt Chart

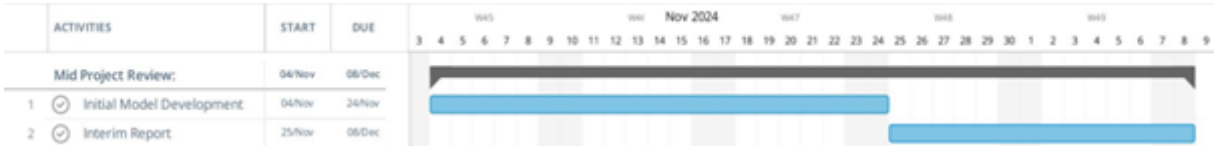

Figure 8.2: Grantt Chart

Figure 8.3: Grantt Chart

Figure 8.4: Grantt Chart

Over the course of this yearlong investigation into Hybrid Quantum–Classical Convolutional Neural Networks (HQCNNs), our trajectory has unfolded in two distinct phases.

The first semester was characterized by smooth progress, rigorous planning, and clear milestones met on schedule. Having laid a solid foundation in quantum machine learning theory and encoding methods, we completed the initial research and design tasks ahead of the mid-project review. During weeks 1–4, we finalized our literature survey on Structured Variational Quantum Circuits (SVQCs), Enhanced Novel Enhanced Quantum Representation (ENEQR), and Fourier Expressivity Analysis (FEA), and in weeks 5–9 we developed and tested a baseline classical CNN to serve as a performance benchmark. By week 11, our first interim report documented a prototype HQCNN which combines a simple ENEQR encoder with a minimal SVQC ansatz with preliminary training runs on MNIST, all achieved within the originally allocated timeline.

This early momentum carried us through the holiday break and into the spring term, where we expanded our prototypes into four distinct HQCNN variants and began Fourier expressivity analyses (FEA). Our codebase matured steadily where positional and intensity encoding modules were fully validated, quantum circuit structures were scripted and simulated via PennyLane's default.qubit, and classical training loops integrated seamlessly. By the end of March, we had demonstrated the first tangible performance gains of SVQCs over random ansätze, adhering closely to our Gantt-chart targets.

However, as the calendar turned to April and we shifted focus to scaling our experiments, we encountered significant computational issues. The very hybrid architectures that promised quantum advantage now imposed huge computational time cost. Each additional qubit in our ENEQR encoder or each extra layer of entangling gates drove simulation runtimes from minutes into hours per epoch. For several weeks, we searched for faster state encoding, reduced-precision arithmetic, parameter sharing schemes, but each promising idea required extensive refactoring and produced only slight speedups.

These computational delays cascaded into our schedule: the planned hyperparameter sweeps and CIFAR-10 experiments slipped well beyond our original deadlines. We decided to refocus on MNIST to complete FEA within the available runtime. While this enabled us to collect expressivity metrics for all four HQCNN versions, it forced us to defer work on more complex datasets and on advanced pruning strategies informed by FEA.

References

Al-Saffar, A. A. M., Tao, H., & Talab, M. A. (2017). Review of deep convolution neural network in image classification. In *2017 international conference on radar, antenna, microwave, electronics, and telecommunications (icramet)* (p. 26-31). doi: 10.1109/ICRAMET.2017.8253139

Amin, M. H., Andriyash, E., Rolfe, J., Kulchytskyy, B., & Melko, R. (2018, May). Quantum boltzmann machine. *Phys. Rev. X*, *8*, 021050. Retrieved from https://link.aps.org/doi/10.1103/PhysRevX.8.021050 doi: 10.1103/PhysRevX.8.021050

Anschuetz, E. R., & Kiani, B. T. (2022). Quantum variational algorithms are swamped with traps. *Nature Communications*, *13*(1), 7760. Retrieved from https://doi.org/10.1038/s41467-022-35364-5 doi: 10.1038/s41467-022-35364-5

Arthur, D., & Date, P. (2022). Hybrid quantum-classical neural networks. In *2022 ieee international conference on quantum computing and engineering (qce)* (p. 49-55). doi: 10.1109/QCE53715.2022.00023

Biamonte, J., Wittek, P., Pancotti, N., Rebentrost, P., Wiebe, N., & Lloyd, S. (2016, 11). Quantum machine learning. *Nature*, *549*. doi: 10.1038/nature23474

Cerezo, M., Verdon, G., Huang, H.-Y., Cincio, L., & Coles, P. J. (2022, Sep). Challenges and opportunities in quantum machine learning. *Nature Computational Science*, *2*(9), 567–576. doi: https://doi.org/10.1038/s43588-022-00311-3

Chen, L., Li, S., Bai, Q., Yang, J., Jiang, S., & Miao, Y. (2021). Review of image classification algorithms based on convolutional neural networks. *Remote Sensing*, *13*(22). Retrieved from https://www.mdpi.com/2072-4292/13/22/4712 doi: 10.3390/rs13224712

Chen, S. Y.-C. (2024). *Evolutionary optimization for designing variational quantum circuits with high model capacity.* Retrieved from https://arxiv.org/abs/2412.12484

Cloirec, H. (2023). Challenges in large-scale optimization: Handling big data and high dimensionality. *Global Journal of Technology Optimization*, *14*, 352.

Cong, I., Choi, S., & Lukin, M. D. (2019, Aug). Quantum convolutional neural networks. *Nature Physics*, *15*(12), 1273–1278. doi: https://doi.org/10.1038/s41567-019-0648-8

Fan, F., Shi, Y., Guggemos, T., & Zhu, X. X. (2024). Hybrid quantum-classical convolutional neural network model for image classification. *IEEE Transactions on Neural Networks and Learning Systems*, *35*(12), 18145-18159. doi: 10.1109/TNNLS.2023.3312170

Farhi, E., Goldstone, J., & Gutmann, S. (2014). *A quantum approximate optimization algorithm.* Retrieved from https://arxiv.org/abs/1411.4028

Gill, S. S., Cetinkaya, O., Marrone, S., Claudino, D., Haunschild, D., Schlote, L., ... Ramamohanarao, K. (2024). *Quantum computing: Vision and challenges.* Retrieved from https://arxiv.org/abs/2403.02240

Gogeissl, M., Safi, H., & Mauerer, W. (2024, June). Quantum data encoding patterns and their consequences. In *Proceedings of the workshop on quantum computing and quantum-inspired technology for data-intensive systems and applications (q-data '24)* (p. 11 Pages). New York, NY, USA: Association for Computing Machinery. doi: 10.1145/3665225.3665446

Gong, L.-H., Pei, J.-J., Zhang, T.-F., & Zhou, N.-R. (2024). Quantum convolutional neural network based on variational quantum circuits. *Optics Communications*, *550*, 129993. Retrieved from https://www.sciencedirect.com/science/article/pii/S0030401823007411 doi: https://doi.org/10.1016/j.optcom.2023.129993

Haque, M. E., Paul, M., Ulhaq, A., & Debnath, T. (2023). Advanced quantum image representation and compression using a dct-efrqi approach. *Scientific Reports*, *13*, 4129. Retrieved from https://doi.org/10.1038/s41598-023-30575-2 doi: 10

.1038/s41598-023-30575-2

Huang, H.-Y., Broughton, M., Mohseni, M., Babbush, R., Boixo, S., Neven, H., & McClean, J. R. (2021, May). Power of data in quantum machine learning. *Nature Communications*, *12*(1). doi: https://doi.org/10.1038/s41467-021-22539-9

Huembeli, P., & Dauphin, A. (2021, February). Characterizing the loss landscape of variational quantum circuits. *Quantum Science and Technology*, *6*(2), 025011. Retrieved from http://dx.doi.org/10.1088/2058-9565/abdbc9 doi: 10.1088/2058-9565/abdbc9

Jeong, S.-G., Do, Q.-V., Hwang, H.-J., Hasegawa, M., Sekiya, H., & Hwang, W.-J. (2023). Hybrid quantum convolutional neural networks for uwb signal classification. *IEEE Access*, *11*, 113726–113739. doi: https://doi.org/10.1109/access.2023.3323019

Kashif, M., & Shafique, M. (2024). *The dilemma of random parameter initialization and barren plateaus in variational quantum algorithms.* Retrieved from https://arxiv.org/abs/2412.06462

Kieferová, M., & Wiebe, N. (2017, Dec). Tomography and generative training with quantum boltzmann machines. *Physical Review A*, *96*(6). Retrieved from http://dx.doi.org/10.1103/PhysRevA.96.062327 doi: 10.1103/physreva.96.062327

Kobayashi, M., Nakaji, K., & Yamamoto, N. (2022). Overfitting in quantum machine learning and entangling dropout. *Quantum Machine Intelligence*, *4*, 30. doi: 10.1007/s42484-022-00087-9

Larocca, M., Thanasilp, S., Wang, S., et al. (2025). Barren plateaus in variational quantum computing. *Nature Reviews Physics*, *7*, 174–189. Retrieved from https://doi.org/10.1038/s42254-025-00813-9 doi: 10.1038/s42254-025-00813-9

Lecun, Y., Bottou, L., Bengio, Y., & Haffner, P. (1998). Gradient-based learning applied to document recognition. *Proceedings of the IEEE*, *86*(11), 2278-2324. doi: 10.1109/5.726791

Liu, B., Ortiz, M., & Cirak, F. (2024, December). Towards quantum computational mechanics. *Computer Methods in Applied Mechanics and Engineering*, *432*, 117403. Retrieved from http://dx.doi.org/10.1016/j.cma.2024.117403 doi: 10.1016/

j.cma.2024.117403

Liu, H., Gao, Y., Shi, L., Wei, L., Shan, Z., & Zhao, B. (2023). Hm-qcnn: Hybrid multi-branches quantum-classical neural network for image classification. In X. Yang et al. (Eds.), *Advanced data mining and applications* (pp. 139–151). Cham: Springer Nature Switzerland.

Lloyd, S., Mohseni, M., & Rebentrost, P. (2014, July). Quantum principal component analysis. *Nature Physics*, *10*(9), 631–633. Retrieved from http://dx.doi.org/10.1038/nphys3029 doi: 10.1038/nphys3029

Marshall, S. C., Gyurik, C., & Dunjko, V. (2023, August). High Dimensional Quantum Machine Learning With Small Quantum Computers. *Quantum*, *7*, 1078. Retrieved from https://doi.org/10.22331/q-2023-08-09-1078 doi: 10.22331/q-2023-08-09-1078

Martín-Guerrero, J. D., & Lamata, L. (2022, Jan). Quantum machine learning: A tutorial. *Neurocomputing*, *470*, 457–461. doi: https://doi.org/10.1016/j.neucom.2021.02.102

Mhiri, H., Monbroussou, L., Herrero-Gonzalez, M., Thabet, S., Kashefi, E., & Landman, J. (2024). *Constrained and vanishing expressivity of quantum fourier models.* Retrieved from https://arxiv.org/abs/2403.09417

Nagata, K., Diep, D., & Nakamura, T. (2022). Computational complexity in high-dimensional quantum computing. *Quantum Machine Intelligence*, *4*, 26. doi: 10.1007/s42484-022-00084-y

Nasr, N., Younes, A., & Elsayed, A. (2021). Efficient representations of digital images on quantum computers. *Multimedia Tools and Applications*, *80*, 34019–34034. doi: 10.1007/s11042-021-11355-4

Oh, S., Choi, J., & Kim, J. (2020). A tutorial on quantum convolutional neural networks (qcnn). In *2020 international conference on information and communication technology convergence (ictc)* (p. 236-239). doi: 10.1109/ICTC49870.2020.9289439

Osorio, S. L. J., Ruiz, M. A. R., Mendez-Vazquez, A., & Rodriguez-Tello, E. (2024). *Fourier series guided design of quantum convolutional neural networks for enhanced*

time series forecasting. Retrieved from https://arxiv.org/abs/2404.15377

Parmar, S. J., Parmar, V. R., Verma, J., Roy, S., & Bhattacharya, P. (2023). Quantum computing: Exploring superposition and entanglement for cutting-edge applications. In *2023 16th international conference on security of information and networks (sin)* (p. 1-6). doi: 10.1109/SIN60469.2023.10474803

Phuc, L. Q., Dong, F., Yoshinori, A., & Kaoru, H. (2009). Flexible representation of quantum images and its computational complexity analysis.. Retrieved from https://api.semanticscholar.org/CorpusID:119005700

Qi, H., Xiao, S., Liu, Z., et al. (2024). Variational quantum algorithms: fundamental concepts, applications and challenges. *Quantum Information Processing*, *23*, 224. doi: 10.1007/s11128-024-04438-2

Ranga, D., Rana, A., Prajapat, S., Kumar, P., Kumar, K., & Vasilakos, A. V. (2024). Quantum machine learning: Exploring the role of data encoding techniques, challenges, and future directions. *Mathematics*, *12*(21). Retrieved from https://www.mdpi.com/2227-7390/12/21/3318 doi: 10.3390/math12213318

Rath, M., & Date, H. (2024). Quantum data encoding: a comparative analysis of classical-to-quantum mapping techniques and their impact on machine learning accuracy. *EPJ Quantum Technology*, *11*, 72. Retrieved from https://doi.org/10.1140/epjqt/s40507-024-00285-3 doi: 10.1140/epjqt/s40507-024-00285-3

Rizvi, S. M. A., Ulum, M. S., Asif, N., & Shin, H. (2023). Neural networks with variational quantum circuits. In N.-S. Vo & H.-A. Tran (Eds.), *Industrial networks and intelligent systems* (pp. 203–214). Cham: Springer Nature Switzerland.

Schuld, M., Sweke, R., & Meyer, J. J. (2021, Mar). Effect of data encoding on the expressive power of variational quantum-machine-learning models. *Phys. Rev. A*, *103*, 032430. Retrieved from https://link.aps.org/doi/10.1103/PhysRevA.103.032430 doi: 10.1103/PhysRevA.103.032430

Senokosov, A., Sedykh, A., Sagingalieva, A., Kyriacou, B., & Melnikov, A. (2024, Mar). Quantum machine learning for image classification. *Mach. Learn.: Sci. Technol*, *5*, 15040. doi: https://doi.org/10.1088/2632-2153/ad2aef

Singhal, P., & Joshi, P. (2024). Advance quanvolutional layers in quantum classical hybrid neural networks for image processing. In *2024 10th international conference on control, automation and robotics (iccar)* (p. 47-52). doi: 10.1109/ICCAR61844.2024.10569440

Suzuki, T., Hasebe, T., & Miyazaki, T. (2024). Quantum support vector machines for classification and regression on a trapped-ion quantum computer. *Quantum Machine Intelligence*, *6*, 31. doi: 10.1007/s42484-024-00165-0

Tilly, J., Chen, H., Cao, S., Picozzi, D., Setia, K., Li, Y., ... Tennyson, J. (2022, November). The variational quantum eigensolver: A review of methods and best practices. *Physics Reports*, *986*, 1–128. Retrieved from http://dx.doi.org/10.1016/j.physrep.2022.08.003 doi: 10.1016/j.physrep.2022.08.003

Volkoff, T., & Coles, P. J. (2021, January). Large gradients via correlation in random parameterized quantum circuits. *Quantum Science and Technology*, *6*(2), 025008. Retrieved from http://dx.doi.org/10.1088/2058-9565/abd891 doi: 10.1088/2058-9565/abd891

Vu, T., Le, L., & Pham, T. (2024). Exploring the features of quanvolutional neural networks for improved image classification. *Quantum Machine Intelligence*, *6*, 29. doi: 10.1007/s42484-024-00166-z

Wang, A., Hu, J., Zhang, S., et al. (2024). Shallow hybrid quantum-classical convolutional neural network model for image classification. *Quantum Information Processing*, *23*, 17. doi: 10.1007/s11128-023-04217-5

Wang, Y., & Luo, Y. (2024). Resource-efficient quantum principal component analysis. *Quantum Sci. Technol.*, *9*(3), 035031. doi: 10.1088/2058-9565/ad466c

Wiedmann, M., Periyasamy, M., & Scherer, D. D. (2024). *Fourier analysis of variational quantum circuits for supervised learning.* Retrieved from https://arxiv.org/abs/2411.03450

Wu, C.-H., & Yen, C.-C. (2024). The expressivity of classical and quantum neural networks on entanglement entropy. *The European Physical Journal C*, *84*, 192. Retrieved from https://doi.org/10.1140/epjc/s10052-024-12558-3 doi: 10

.1140/epjc/s10052-024-12558-3

Wu, Y., Yao, J., Zhang, P., & Zhai, H. (2021, August). Expressivity of quantum neural networks. *Physical Review Research*, *3*(3). Retrieved from http://dx.doi.org/10.1103/PhysRevResearch.3.L032049 doi: 10.1103/physrevresearch.3.l032049

Xu, Z., Shen, K., Cai, P., et al. (2024). Parallel proportional fusion of a spiking quantum neural network for optimizing image classification. *Applied Intelligence*, *54*, 11876–11891. doi: 10.1007/s10489-024-05786-3

Yi, Z., Liang, Y., & Situ, H. (2024). *Enhancing variational quantum circuit training: An improved neural network approach for barren plateau mitigation.* Retrieved from https://arxiv.org/abs/2411.09226

You, X., & Wu, X. (2021). *Exponentially many local minima in quantum neural networks.* Retrieved from https://arxiv.org/abs/2110.02479

Younesi, A., Ansari, M., Fazli, M., Ejlali, A., Shafique, M., & Henkel, J. (2024). *A comprehensive survey of convolutions in deep learning: Applications, challenges, and future trends.* Retrieved from https://arxiv.org/abs/2402.15490

Zaman, K., Ahmed, T., Hanif, M. A., Marchisio, A., & Shafique, M. (2024). *A comparative analysis of hybrid-quantum classical neural networks.* Retrieved from https://arxiv.org/abs/2402.10540

Zeng, B., Chen, X., Zhou, D.-L., & Wen, X.-G. (2019). Correlation and entanglement. In *Quantum information meets quantum matter: From quantum entanglement to topological phases of many-body systems* (pp. 3–35). New York, NY: Springer New York. Retrieved from https://doi.org/10.1007/978-1-4939-9084-9_1 doi: 10.1007/978-1-4939-9084-9_1

Zhang, Y., Lu, K., Gao, Y., et al. (2013). Neqr: a novel enhanced quantum representation of digital images. *Quantum Information Processing*, *12*, 2833–2860. doi: 10.1007/s11128-013-0567-z

Zhuang, J., Cunningham, J., & Guan, C. (2024). *Improving trainability of variational quantum circuits via regularization strategies.* Retrieved from https://arxiv.org/abs/2405.01606